CHALMERS

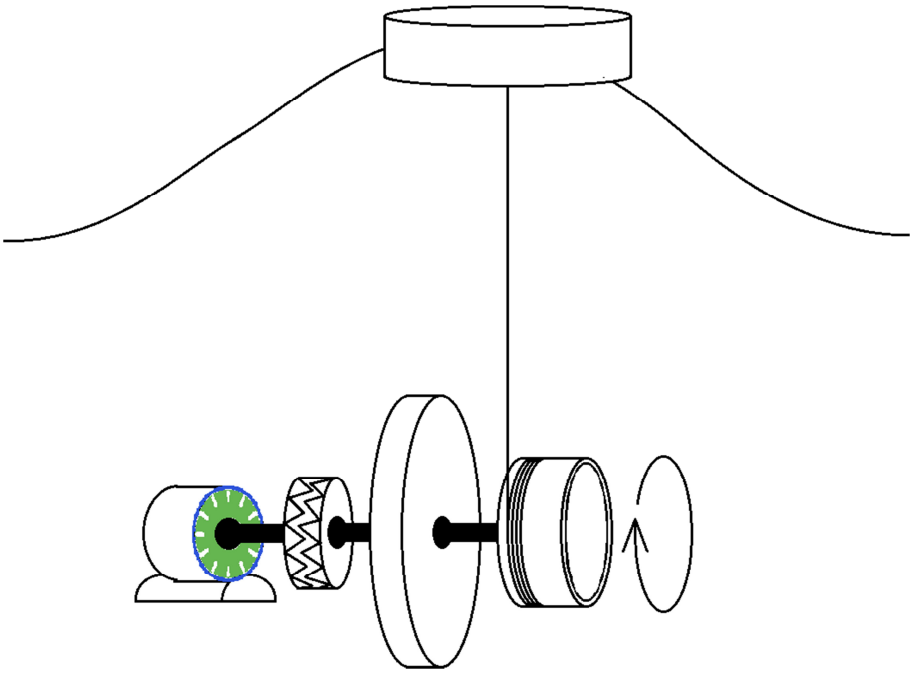

Investigation of a wave energy converter with a flywheel and a corresponding generator design

Thesis for the degree of Master of Science in Electrical Engineering

KIM LARSSON

Division of Electric Power Engineering
Department of Energy and Environment
CHALMERS UNIVERSITY OF TECHNOLOGY
Göteborg, Sweden, 2012

Investigation of a wave energy converter with a flywheel and a corresponding generator design

KIM LARSSON

Division of Electric Power Engineering

Department of Energy and Environment

CHALMERS UNIVERSITY OF TECHNOLOGY

Göteborg, Sweden, 2012

Investigation of a wave energy converter with a flywheel and a corresponding generator design
KIM LARSSON

Division of Electric Power Engineering
Department of Energy and Environment
Chalmers University of Technology
SE-412 96 Göteborg
Sweden
Telephone + 46 (0)31-772 1000

Cover:
System overview of the wave energy converter and generator investigated in this thesis. Buoy floating on a wave connected via line to a freewheel. Freewheel drives axis connected to flywheel, gear box and generator.

This report is written in LaTeX

Printed by Chalmers Reproservice
Göteborg, Sweden, June 2012

Abstract

A wave energy converter (WEC) with a flywheel have been investigated and suitable generator designs have been proposed and compared. From the uptake of energy from the waves via a buoy to the conversion of mechanical to electrical energy in a generator, this thesis focuses on connecting all the steps on the way. The vertical motion of a buoy, being moved upwards by a wave, exerts a pulling force on a line that connects the buoy to a freewheel; the motion translates to a rotational motion around the axis of the freewheel. The axis connects to a flywheel with a rotational inertia, a gear box and finally a generator. The whole system, except for the buoy, is placed at the bottom of the sea. A 3 meters high and 5 seconds long wave together with an assumed current density for the generator, gives the input data for the generator design. Depending on the use of a flywheel with a large rotational inertia or not and which control strategy is used, the size of the generator vary between a diameter and length of 300 and 410 mm, whilst the maximum electric torque vary between 1350 and 2900 Nm.

Acknowledgements

First I would like to thank my supervisor Christian Du-Bar who has patiently answered all my questions or guided me to the right person at the department. The discussions I had with him has shaped this thesis and the resulting outcome. Secondly, my examiner Sonja Lundmark for answering questions and giving me important as well as interesting thoughts and facts both by word and through literature. I would also like to thank both Christian and Sonja for their effort put in proofreading and helping me structuring the report.

Furthermore, I would like to acknowledge the inventor behind the WEC design that made this thesis work possible, Per Jakobsson. Among other things, Per collected the necessary wave data for this thesis work which saved me a lot of time. The regular meetings had with Per, Sonja and Christian motivated me and brought my work forward. A big thanks also to all helpful and encouraging people here at the department of Electric Power Engineering.

Finally, I would like to thank my friends and family for the never faltering love, support and encouragement you have given me. Also that you never stopped believe in my work, which I sometimes did.

Contents

1 Introduction

1.1 Background

The ever growing increase in energy demand all over the world together with the requirement for renewable and environmental friendly energy, brings forth the long-known but not fully explored ocean wave energy as an energy source with great potential. Wave energy is at the moment very unexploited, in Norway and Sweden alone there are plenty of coast that is suitable for wave energy converters (WECs). There is also a very big world market where the competition still is quite small since both product and market exist in an early state of development. As of yet there are no WECs that works optimal in all kinds of waves and seas, which makes the competition markets smaller, e.g. some companies compete for the wave energy outside the coast of Scotland, others Norway's coast and some Sweden's etc.

In this thesis will an innovative WEC's potential be investigated to see if it has a chance to reach the commercial market inside the environmental friendly energy sector. This is a step in Per Jakobsson's work to develop a prototype that later shall be patented. He wants to obtain information that will give an indication of whether this converter may produce more or less electricity than already existing WECs.

1.2 Previous work

In the early spring of 2002, researchers and graduate students at the department of electrical theory at Uppsala university began to plan the project *Lysekilsprojektet*. Only four years later, just outside Gullholmen, was the first linear generator installed at the bottom of the sea, connected to a buoy and started producing electricity [1]. They are using a WEC from *Seabased* [2], consisting of a linear generator connected to a buoy at the surface. The kinetic energy of the wave is transferred to the buoy during a wave front and is later converted to electrical energy in the generator. Approximately 20% of the incoming energy of the wave can be absorbed in this installation [1]. The translator is made of very strong permanent magnets (NdFeB magnets) and is moving up and down inside the linear generator as the buoy is vertically moved by the waves. This makes it possible to induce high voltages, of about 100 V in the coils of the stator, even though the velocity of the translator is low. The resulting power peaks are between 10 and 15 kW. Since it is a linear generator, the translator has two end positions. The first position is reached when either the buoy cannot pull the translator higher because the buoy is at the peak of the wave, or when the translator is at the top of the linear generator and hence is stopped by the upper end stop. The second position is when the buoy has a negative vertical velocity and the translator reaches the bottom of the generator as a spring pulls it down. This linear operation mode produces pulses of energy, that may have quite high peaks that are difficult to utilize compared to a steady power output that is more easily utilized and gives higher efficiency.

The utilization rate is a measure of how much of the time the WEC is exposed to waves it can generate electricity from. For WECs in Sweden, this rate is between 35% and 50%

of the time, but can in greater oceans be as big as 70% of the time. This means that the WEC performs useful work for 70% of the time and is idle for 30% of the time.[1]

The general idea is then to connect tens of generators together into WEC farms, in much the same way as wind farms, converting the mechanical energy to electrical energy which can be delivered to the electrical grid.

For further information about research and companies in the WEC industry there is an organization called Ocean Energy Centre (OEC)[3], that is administered by Chalmers University of Technology.

1.3 Objective

The main objective of this work is to create a control model that simulates waves and the lifting force on a buoy in it, as well as to investigate different control strategies of the WEC, regarding the output effect and total energy uptake for a certain wave. The last objective is to make a comparison between three different synchronous generator (SG) designs suitable for the invented WEC.

1.4 Methods

Four control strategies will be implemented in *Simulink* and the results from these four will provide the input data to the generator design. An analytic design program, *RMxprt*, will be used to make a permanent magnet synchronous generator (PMSG) design. Then will transient analyses in 2D be performed in the finite element analysis program *Maxwell*. Results regarding the maximum electric torque and size of the generator will thus be had.

1.5 Limitations

Since this master thesis is of electro technical nature, the mechanics needed will be approximated with simplified expressions. The outline and design of the buoy will not be treated here, an already tested design from *Lysekilsprojektet*, which is decribed in reference [4], will be used.

1.6 Scope

This thesis is divided into two major parts. The first regarding the design of a WEC controller and the second regarding the design of a permanent magnet synchronous generator (PMSG). Both have their corresponding theory chapters and both are summed up in the discussion and conclusion chapters.

Chapter 1 gives a short presentation to wave energy and WECs. Previous work in the field is given through a short summary of *Lysekilsprojektet*. The purpose and results that are aimed for are also given.

Chapter 2 explains the theory of the WEC. It describes the different parts in the system and how the wave energy is converted to a torque that is fed to the generator.

Chapter 3 contains the theory about PMSG and explains how the key design parameters are decided when designing the PMSG in chapter 5.

Chapter 4 shows how the WEC control model was made. It contains overviews of the implemented *Simulink* block schemes and explains how the model is controlling the flow of energy from the wave front to the generator during a wave period.

Chapter 5 describes the PMSG design, which parameters that were assumed and approximated and which were calculated and swept. The swept parameters where chosen to be optimized for efficiency and a magnetic flux density close to 1.2 T.

Chapters 6, 7 and 8 sums up the report by discussing the results from chapters 4 and 5. A conclusion is made and what could have been done with more time is discussed in the future work part.

2 Waves and wave energy converters

The uptake of wave energy can be made according to the system in figure 2.1. In this thesis is the first part, from the buoy to the gear box, referred to as the WEC and the second part as the generator. The WEC is divided into four parts; buoy, freewheel, flywheel and gear box, just for the illustration of how the system is constructed. Integrating the three latter parts could be practical from a manufacturer point of view, but not as convenient as an explanatory scheme. The whole construction, except for the buoy, is placed at the bottom of the sea.

When the buoy is displaced relative to the water surface, during a wave front, a pulling force is exerted on the line that connects the buoy to the freewheel. The freewheel starts to rotate and drives the axis when it has the same or higher velocity than the flywheel. The flywheel is a rotational inertia, which is able to store energy. The freewheel thus drives the flywheel and the generator, the latter via the gear box, during a wave front. At the gear box, the angular velocity, ω_1, at the flywheel side of the axis is increased with a ratio of G as the torque, τ_1, is decreased G times, to become ω_2 and τ_2 at the generator side, respectively. The generator converts the mechanical energy to electrical energy. When the wave front is over there is no force exerted on the line. The freewheel turns back to its original position and awaits a new wave front. Meanwhile, the mechanical energy which is stored in the flywheel is transferred to the generator, via the gear box.

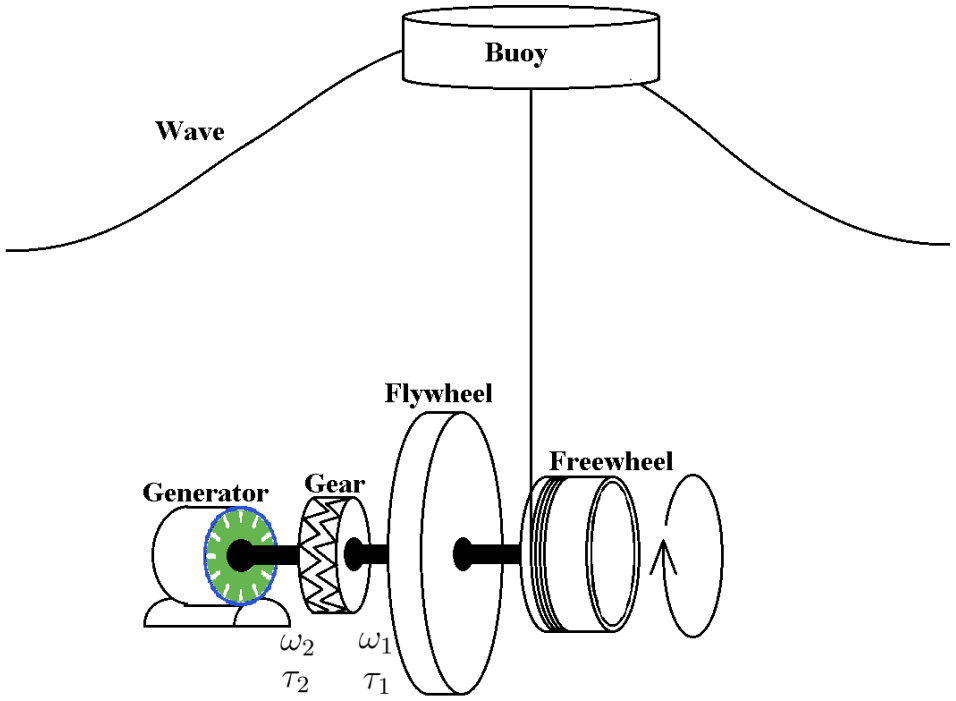

Figure 2.1: System overview of the wave energy converter and the generator.

2.1 Waves

Waves at sea are very energy dense, much more than both wind and solar. According to *Seabased* [2] is the energy density per meter wave, for a wave of two meter in amplitude, about ten times more than the energy density of wind per square meter. Lengths and amplitudes of waves vary quite a bit over the world and hence it is important to know for which waters a WEC should be designed. This design is primarily meant for Sweden's west coast and the coast of Norway, but can most certainly be adjusted to work at the coast of Scotland for example. The average energy per meter of wave in Sweden is about 5-10 kW/m and 20-80 kW/m in Norway [2].

The waves on the Swedish west coast are between zero and seven meters in amplitude and two to twelve seconds in length [5]. Even though the most common waves are barely one meter high and between two to five seconds long, these are not the ones that hold the most energy. Waves between one and four meters high and four and seven seconds long hold the most energy. One strategy is therefore to design the WEC for these waves.

2.2 Wave energy converters

The WEC shown in figure 2.1 is designed with a freewheel to always have the rotational motion of the axis and hence the generator in one and the same direction. The freewheel have many turns of line wound around it, thus it can deal with different wave amplitudes, since several meters of line easily can be wound around the wheel and hence be pulled out as the buoy rises towards the surface during a wave front. When the buoy has reached the top of the wave and starts descending the line slacks and the freewheel decouples. The freewheel retracts the line to its starting position and awaits a new pull from the buoy. This without affecting the rotational motion of the axis.

The freewheel is only connected to the axis of rotation while it has the same speed as the flywheel. The flywheel however, is always connected to the axis as well as to the primary side of the gear box. It can thus store the energy not used by the generator during a wave front. This in order to decrease the peak load power or torque on the generator and possibly reduce the size of the generator.

The gear box is always connected to the axis with a gear shift between its primary and secondary sides, i.e. the primary side connects to the flywheel and the secondary side to the generator. The gear box is needed in order to reduce the torque from the flywheel, this in order to have a smaller generator than without a gear box. Thus is an increase in angular velocity obtained.

2.2.1 Existing WECs

WECs today are usually operating with a linear motion, like the WEC in this report, and a linear generator, like the one used by *Seabased* [2]. The system made by *Seabased* has a buoy at the surface which, via a line, is connected to a generator at the bottom of the sea. Thus, it is usually placed at shallow waters.

Waves4power also uses a linear motion, but has a linear generator that is integrated in the buoy [6]. Thus it can be placed at shallow as well as deep waters.

There is also *Minesto* [7], that make use of the tidal currents with a construction that surfs on the currents in a horizontal eight. These WECs are operating completely under water and does not disturb the water surface.

Oceanharvesting offers a design with a sinker, which has a similar use as the flywheel in figure 2.1. It is a big buoy with a built-in generator that is able to float on both the top of a wave and the valley between two waves at the same time due to its size. It stores wave energy in a sinker by pulling it up and then transfer energy to the generator by letting it back down [8].

2.3 Physical principles of the WEC

2.3.1 Lifting force

The lifting force acting on the buoy in figure 2.1 was calculated for the dimensions of the buoy found in [4], which has a height, h_{buoy}, of 0.8 m, a radius, r_{buoy}, of 1.5 m and a weight, m_{buoy}, of approximately 1 tonne. Archimedes principle states that the force acting on an object submerged in a fluid is equal to the weight of the, by the object, displaced fluid. Therefore is the lifting force, F_{buoy}, acting on the buoy dependent on how much of the buoy is submerged in water, $V_{water} = V_{buoy,submerged}$, see Eq. (2.1).

$$\begin{aligned} F_{over} &= (m_{water} - m_{buoy})g = (\rho_{water} V_{water} - m_{buoy})g \\ &= (\rho_{water}\pi h_{submerged} r_{buoy}^2 - m_{buoy})g \quad \text{for } 0 < h_{submerged} < h_{buoy} \end{aligned} \tag{2.1}$$

F_{over} is the lifting force acting on the buoy when the buoy is not entirely submerged, m_{water} is the weight of the water being pushed aside by the submerged part of the buoy, ρ_{water} is the density of water, $h_{submerged}$ is how deep the buoy is submerged in water (from the bottom of the buoy to the surface) and g is the gravitational acceleration constant. When the buoy is fully submerged under water or yet deeper under water, (2.1) does not apply. For this interval, Eq. (2.2) is needed, since it shows how the lifting force, F_{under}, increases due to increased pressure under water.

$$\begin{aligned} F_{under} &= (m_{water}(\frac{h_{under}}{h_2} + 1) - m_{buoy})g \\ &= (\rho_{water}\pi h_{buoy} r_{buoy}^2(\frac{h_{under}}{h_2} + 1) - m_{buoy})g \quad \text{for } 0 < h_{under} < h_2 \end{aligned} \tag{2.2}$$

h_{under} is how deep the buoy is submerged in water (from the surface to the top of the buoy) and h_2 is the depth where the pressure and hence the lifting force is double that at the surface.

2.3.2 Combination of linear and rotational motion

The lifting force is converted to torque as the vertical motion of the line connected to the buoy translates to a rotational motion around the axis of the freewheel, with a radius r_{fw}, see (2.3).

$$\tau = r_{fw} F_{buoy} \sin(\theta) = r_{fw} F_{buoy} \tag{2.3}$$

$\sin(\theta) = 1$ since the pulling motion of the buoy is assumed to be perpendicular to the imaginary lever arm of the freewheel at all times. The angular velocity of the rotor and hence the freewheel is needed in order to calculate the mechanical power in to the generator. The vertical velocity of the buoy is calculated by integrating the vertical acceleration of the buoy, which is calculated as

$$a = \frac{F_{buoy}}{m_{buoy}} \tag{2.4}$$

The angular acceleration of the freewheel is then calculated as

$$\alpha = \frac{F_{buoy}}{m_{buoy} r_{fw}} \tag{2.5}$$

The vertical velocity is converted to angular velocity in much the same way as force to torque, see (2.6).

$$\omega = \underbrace{v}_{m/s} \underbrace{\frac{360}{2\pi r_{fw}}}_{^\circ/m} \underbrace{\frac{\pi}{180}}_{rad/^\circ} = \frac{v}{r_{fw}} \tag{2.6}$$

The mechanical power from the buoy to the flywheel is calculated as

$$P_{mec} = r_{fw} F_{buoy} \frac{v}{r_{fw}} = \tau\omega \tag{2.7}$$

The mechanical power in to the generator, via a lossless gear box, is the same

$$P_{mec} = \frac{\tau}{G} \omega G = \tau\omega \tag{2.8}$$

2.3.3 Flywheel

A flywheel is used to store energy, but it also smooths out power variances. To be able to do this it has to have a certain rotational inertia, J, which is specifically chosen for the application at hand. Since J depends on both size, shape and mass of the object rotating around an axis, the same J can be had with lots of different configurations of these three parameters. Disregarding the shape, since the cylindrical shape is the only one used here,

one can see the dependencies of the size by the height, h, and the radii, r_{out} and r_{in}, and mass, m, in (2.9) and (2.10). J for the flywheel in figure 2.1 is calculated with (2.9) and J for the rotor of the generator is calculated with (2.10).

The rotational inertia for a solid cylinder $\quad J = \frac{1}{2} m r_{out}^2 = \frac{1}{2} \pi \rho h r_{out}^4$ (2.9)

The rotational inertia for a hollow cylinder

$$J = \frac{1}{2} m (r_{out}^2 + r_{in}^2) = \frac{1}{2} \pi \rho h (r_{out}^2 + r_{in}^2)(r_{out}^2 - r_{in}^2) = \frac{1}{2} \pi \rho h (r_{out}^4 - r_{in}^4) \tag{2.10}$$

The energy stored in a rotating inertia $\quad E = \frac{1}{2} J \omega^2$ (2.11)

Equations (2.9) to (2.11) can be found in [9], where ρ is the density of the object.

The energy stored in a flywheel can be calculated by (2.11), which also shows that the amount of energy, E, stored is quadratically dependent on the angular velocity, ω, while it is linearly dependent on the rotational inertia J. However, the torque applied to or exerted from a flywheel is linearly dependent on the derivative of ω since a torque, positive or negative, only can be achieved by a change in ω according to

$$\tau = J \frac{\partial \omega}{\partial t} \tag{2.12}$$

The torque, τ, is extracted from a flywheel by reducing its ω and thus having a negative angular acceleration

$$\alpha = \frac{\partial \omega}{\partial t} \tag{2.13}$$

If τ is applied to a flywheel, then ω is increased by a positive angular acceleration, α.

The storing of wave energy in the flywheel is only meant to decrease the load on the generator and not for long time storage. The most of the energy stored must be transferred to the generator before the beginning of the next wave front, so that the energy of the next wave front can be stored. The waves are assumed to be relatively constant, which is why the same angular velocity is wanted every time a new wave front is met. The maximum angular velocity possible to maintain in a flywheel is, among others, set by its bearings. At a certain ω the strain on the bearings will become so large that the flywheel possibly will have difficulties maintaining its speed and thus its stored energy.

As the energy possible to be stored in a rotating inertia depends on ω^2, see (2.11), the rotational inertia of the rotor on the secondary side is equivalent to $G^2 J$ on the primary side of the gear box, with the gear G. The energy to be stored is assumed to be the same whether J is placed on the primary or secondary side of the gear box, i.e. a lossless gear box is assumed. This can be confirmed with a simple example, see appendix A.

Whether the flywheel should be placed on the primary or the secondary side of the gear box is beyond the scope of this thesis. Having the flywheel on the primary side results in

a larger rotational inertia than on the other side of the gearbox, but also in a smoothed out and slowly varying τ and ω since the flywheel does not allow for any sudden peaks and changes in either of the two. A possible benefit of having the gear box placed after the flywheel would be a longer life time of the gear box, but placing the flywheel after the gear box would make the flywheel G^2 times smaller.

3 Permanent magnet synchronous generator

A synchronous generator (SG) is a machine that outputs an induced voltage with a frequency linearly dependent on the synchronous speed N_s of the magnetic field exerted by the rotating rotor. According to reference [10], the frequency f of the electric output is dependent on the number of pole-pairs p and N_s, see (3.1).

$$f = \frac{N_s \cdot p}{60} \tag{3.1}$$

A SG with permanent magnets embedded in or attached to the rotor is known as a permanent magnet synchronous generator (PMSG). They have outputs ranging from about 100 W to 100 kW [11].

Using permanent magnets instead of field windings to produce the magnetic flux saves the magnetizing losses that are unavoidable with field windings, but increases the expenses to obtain the magnetic flux linkage Φ. This since the cost of rare earths such as neodymium magnets is by far greater than the cost of the copper used to manufacture field windings and the corresponding magnetizing losses. However, the use of permanent magnets in the rotor gives a very reliable construction, since no external source of power is needed to excite the magnets there is no need for an electric connection to the rotor and as such the construction becomes more sustainable.

If the mechanical movement of the rotor is constant, a constant voltage and frequency will constitute the output, but if the angular velocity of the rotor varies a varying output voltage and frequency will be obtained. Depending on what kind of power electronics are used, the output should be limited to a certain range for a high efficiency. Since converting mechanical power to electrical requires both speed and force or in this case angular velocity and torque, the generator will have a certain electrical torque. This electrical torque is changed by altering the withdrawal of current from the generator. To be able to output a constant voltage and frequency to the grid from a varying voltage and frequency source and controlling the generator, a converter is needed. The constant output can be either AC or DC depending on the connecting grid.

3.1 Stator design

The stator is the stationary part in the generator and in the case of an exterior-rotor configuration it is placed inside the rotor, see figure 3.1.

The stator core is usually made of steel laminations (henceforth referred to as iron core) and its size can be altered by increasing or decreasing the radius of the shaft, its outer diameter, the geometry of the slots or the length of the stator. The magnetic flux density, B, in the stator and the amount of material used can thus be weighed against each other since B is inversely proportional to the cross-sectional area of the magnetic guides, such as the cross-sectional area of the stator teeth and the rotor yoke, A_t and A_r

respectively.

$$B = \frac{\Phi}{A} \tag{3.2}$$

The cross-section of the coils is shown in figure 3.1, where number 6 shows how the coils are wound around the teeth, so that half of each coils cross-sectional area is on either side of the teeth.

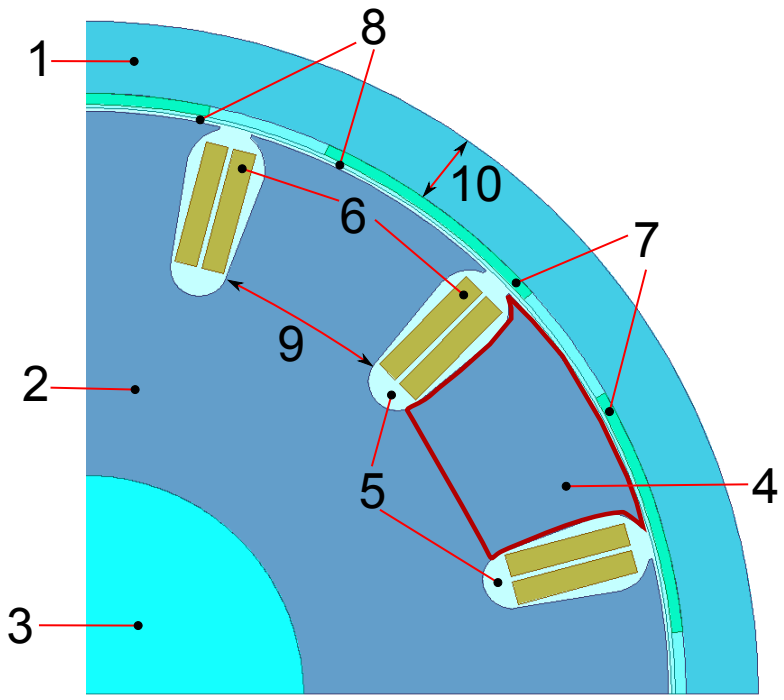

Figure 3.1: A quarter cross-section of the generator design, showing the different parts.

1. Rotor yoke, the rotating part.
2. Stator yoke, the stationary part.
3. Shaft, non-magnetic.
4. Stator tooth.
5. Slots.
6. Coil/armature winding.
7. Permanent magnets.
8. Air gap, between PM and tooth.
9. Narrowest cross-sectional area of tooth A_t.
10. Cross-sectional area of rotor yoke A_r.

3.1.1 Induced voltage

In order to get output power from the generator, an induced voltage is needed. This voltage is created by a relative motion between the magnetic field of the rotor and the armature windings of the stator. The electric circuit of the stator can be described with an equivalent circuit as shown in figure 3.2, where an induced current i is flowing through the series connection of an induced voltage source $v_{induced}$, a conductor resistance R_c and

an output voltage v_{out}. Thus would the output voltage and the current be

$$v_{out} = v_{induced} - iR_c \tag{3.3}$$

$$i = \frac{v_{induced} - v_{out}}{R_c} \tag{3.4}$$

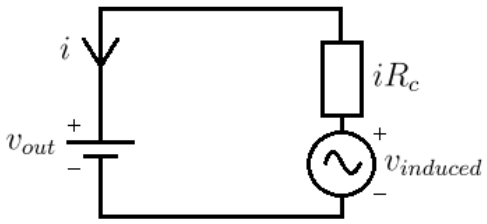

Figure 3.2: Equivalent circuit of the electric stator circuit.

For generator operation, we need a positive current in the direction shown in figure 3.2 and hence $v_{induced} > v_{out}$, which follows naturally since the induced voltage have a voltage drop over R_c. Ideally would $v_{induced} \gg iR_c$ or $R_c = 0$ in order to minimize losses and maximize the output power.

Faraday's law (3.5) explains how the change in flux linkage over time in a conductor induces a voltage in that conductor

$$v_{induced} = \frac{d\phi}{dt} \tag{3.5}$$

The voltage potential $v_{induced}$ in the conductor will drive a current i in that conductor.

3.1.2 Magnetic flux density and flux linkage

The magnetic flux density B is a measure of how much of the iron core in the magnetic circuit that is utilised and the approximation of B being uniform inside any magnetic guide is used in this thesis. In a PMSG, the flux linkage due to the permanent magnets, Φ_M, is responsible for the major part of the flux linkage, hence is the magnetic flux density B in the magnetic guide mainly dependent on Φ_M and the narrowest cross-sectional area A of the magnetic guide, see (3.6). In figure 3.3 the flux linkage is plotted as vectors and the cross-sectional area of the magnetic conductor is shown by the lines with red arrows. A contribution to the total flux linkage Φ comes from the flux linkage Φ_I, which is induced by the stator current. B_M is only dependent on the flux linkage in the magnets and the cross-sectional area of the magnetic guide, but B_I is dependent on the ampere-conductor product IN and the total reluctance $\mathcal{R}$ of the circuit. $\mathcal{R}$ consists of the air gap reluctance $\mathcal{R}_g$ and the reluctance of the magnetic circuit in the iron core $\mathcal{R}_i$.

$$B = \frac{\Phi}{A} = \frac{\Phi_M + \Phi_I}{A} = \frac{\Phi_M}{A} + \frac{IN}{A\mathcal{R}} = \underbrace{\frac{\Phi_M}{A}}_{\text{Magnet, } B_M} + \underbrace{\frac{IN}{A(\mathcal{R}_g + \mathcal{R}_i)}}_{\text{Induced, } B_I} \tag{3.6}$$

The flux linkage in a magnet Φ_m is dependent on the remanent flux linkage of that magnet Φ_r, which is the maximum flux linkage achieved when short-circuiting the magnet. Φ_m also depends on the internal magnet permeance P_{m0} and the air gap reluctance $\mathcal{R}_g$ according to (3.7) [10].

$$\Phi_m = \frac{1}{1 + f_{LKG} P_{m0} R_g} \Phi_r \tag{3.7}$$

$$P_{m0} = \frac{\mu_0 \mu_{rec} A_m}{L_m} \tag{3.8}$$

$$\mathcal{R}_g = \frac{L_g}{\mu_0 A_g} \tag{3.9}$$

f_{LKG} is a constant that is typically 0.95 for machines with surface mounted magnets, μ_0 is the permeability of vacuum, μ_{rec} is the relative permeability of the magnet, A_m is the area of the magnet, L_m the thickness of the magnet, L_g the length of the air gap and A_g the area of the air gap.

Reluctance is the resistance felt by the flux linkage when flowing in a magnetic circuit. Usually, when the iron core is not saturated, the reluctance is much greater in the air gap than in the iron core, so $\mathcal{R}_g \gg \mathcal{R}_i$, even for very small air gaps and long magnetic guides in the iron core.

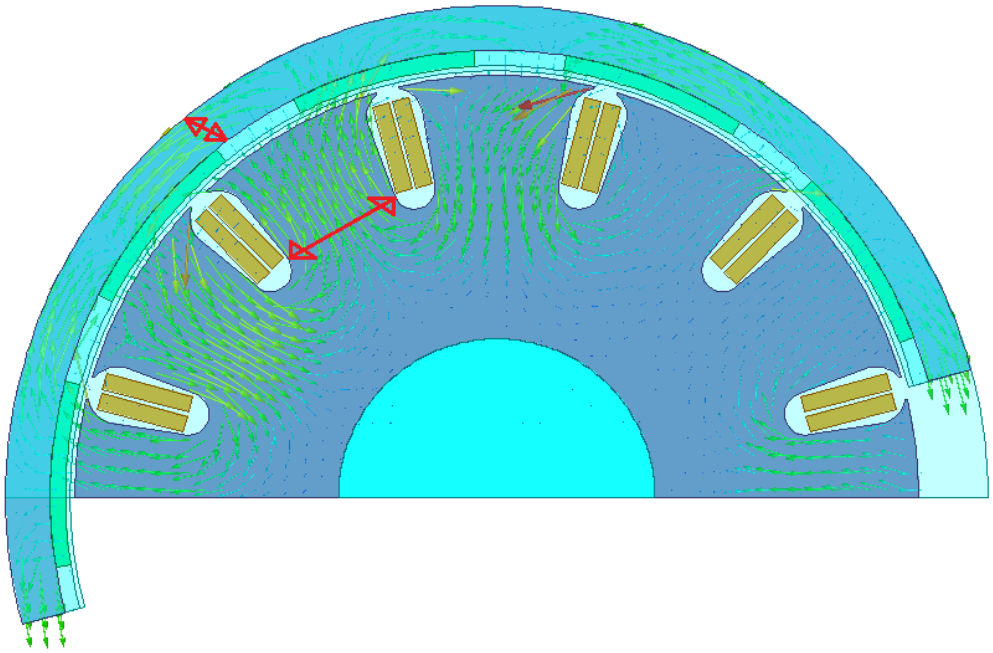

Figure 3.3: The flux linkage direction in the generator.

Magnetic iron starts to saturate at approximately $B_{max} = 1.8$ T, at the knee in the B-H curve seen in figure 3.4. It is important to design a generator that operates well below the saturation level, at typically 1.1 to 1.3 T, and only during short times of overpower is close to or at B_{max}. This is because the reluctance of the iron core, $\mathcal{R}_i$, approximately doubles per 0.1 T increase after the saturation of the iron begins at 1.8 T and $\mathcal{R}_i$ should at all times be kept low to minimize losses.

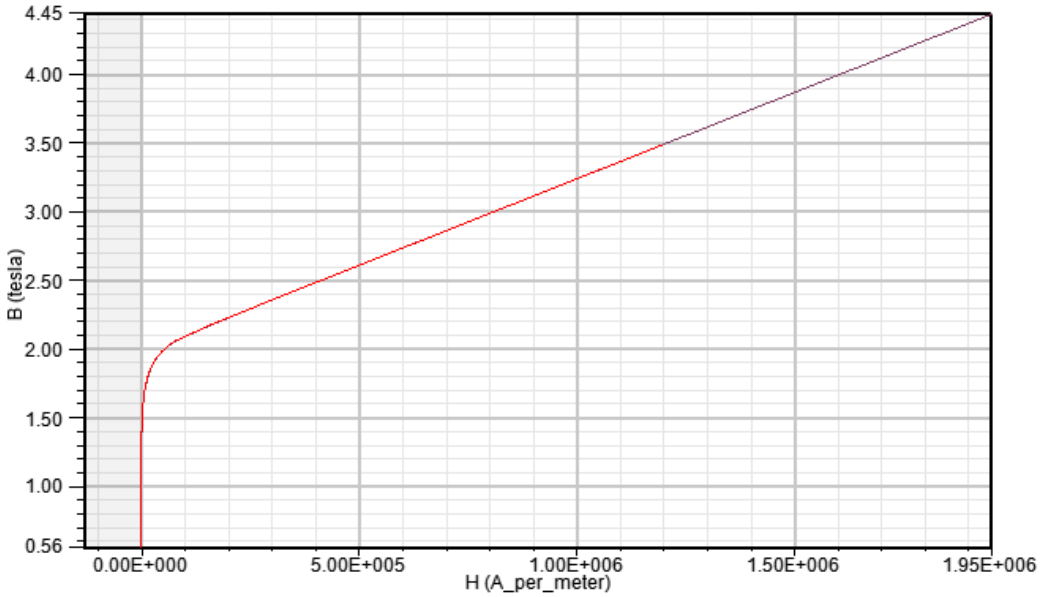

Figure 3.4: B-H curve for steel.

3.1.3 Air gap and slots

The coils are placed in slots instead of being mounted on the surface of the stator in order to get as small air gap as possible. This since a small air gap is important in order to get as much of the flux from the magnets to go through the stator teeth instead of leaking from one pole to the other without crossing the air gap. So by using slots, the flux density in the stator teeth and the rotor yoke can be large without having a large magnetic flux from the magnets.

The magnetic flux from the magnets, see figure 3.3, that flows through the stator teeth or the coils in the stator slots are referred to as the flux linkage. This is the flux that links with the coils that are wound around the teeth and performs the useful work of inducing voltages and currents in the coils. The weighing between how much space the teeth and slots should occupy is another design dilemma, where the last were the weighing between B and A, see section 3.1. Increasing the space that is occupied by the slots decreases the cross-sectional area of the flux path and thus increases the flux density. If instead decreasing the space had by the slots is the flux density decreased.

Since there have to be an integer number of slots per phase and the three phase system is the most suitable, the total amount of slots is always a multiple of three. Due to symmetry, i.e. to achieve a smooth operation, it is however recommended to have a multiple of two slots per phase, thus all slots will have an opposite slot, i.e. a return path. This gives us that the number of slots needed to achieve smooth operation in a three phase system typically is a multiple of six. The slots/pole ratio is another important parameter, which should be close to one but not be one, to achieve smooth operation and thus a low cogging torque [10]. Therefore will the number of poles and slots be close to each other.

The slots are to be shaped for the magnetic flux density and the amount of copper needed, but the narrowest cross-sectional area of a tooth, A_t, should never be so narrow that it causes a $B > B_{max}$.

3.2 Rotor design

The rotational inertia of the rotor can be made either high or low depending on the use of the generator. If the rotor is meant to smooth out a time varying or pulsating torque a large rotational inertia can be used to slow down the mechanical response. For other applications such as servo motors, where a fast response is of interest, it is important to have a small rotational inertia of the rotor. The thickness of the rotor yoke affects the magnetic flux density in the same way as the cross sectional area of the stator teeth in the stator.

The poles, windings or PMs, are positioned symmetrically around the inside of the rotor (for an exterior-rotor configuration). It is common practice to put the windings in slots in the rotor or even embed them inside the rotor yoke during manufacturing, but PMs are usually surface mounted with some kind of adhesive.

3.2.1 Poles

Poles are placed symmetrically and in pairs because the flux flowing out from one pole has to flow in to another pole. Since the poles are placed like this, the radial force acting between a coil and a pole will be the same but opposite to the radial force acting on a pole and coil on the opposite side of the stator. Ideally this results in no net force affecting the rotor radially and only the weaker tangential force will be affecting the rotor.

The surface of the inside of the rotor that is covered with poles, compared to the total surface is referred to as the pole embrace. By letting the poles occupy different amount of space along the inside of the rotor several different shapes of the induced voltage can be obtained.

As mentioned in section 3.1.3, the slots/pole ratio is important when determining the amount of cogging in the machine. If one have an integral slot configuration, i.e. the ratio is an integer, then all the poles will line up with all the slots causing cogging. This is an unwanted operation mode because it generates current peaks, instead of the smooth/constant current that is wanted. If fractional slot configuration is used, then the line up of all poles and slots will never occur, thus giving a much smoother torque.

Poles can be made up of field windings that needs a separate current supply circuit or by permanent magnets (PMs). The PMs are usually made of high coercivity materials such as ferrite or rare-earths, e.g. Neodymium or Samarium-cobalt. The neodymium magnets are the strongest and most cost competitive magnets of the rare-earths.

4 Wave energy converter model

In the first section of this chapter, the model and implementation of how the lifting force of the buoy depends on the vertical position of the buoy in a wave is described; in the following sections the resulting behaviour of the buoy when being controlled is presented.

Figure 4.1 shows how the control model is divided into three different parts; *time delay*, *wave front* and *flywheel operation*. The buoy is controlled to maximize the energy uptake from the wave front for four different control strategies. The chapter is concluded with the presentation of three different cases and the dimensioning of them in order to get a low maximum electric torque and as constant electric torque as possible.

As with most analytical models there are approximations and assumptions. In this case a buoy with height $h_{buoy} = 0.8$ m and radius $r_{buoy} = 1.5$ m is used. The model only take into consideration how deep the buoy lies in the water corresponding to a buoy that lies equally deep across its entire body. This even though a wave can be shorter than the buoy is wide. The viscous damping of the buoy as it moves through the water, is also neglected.

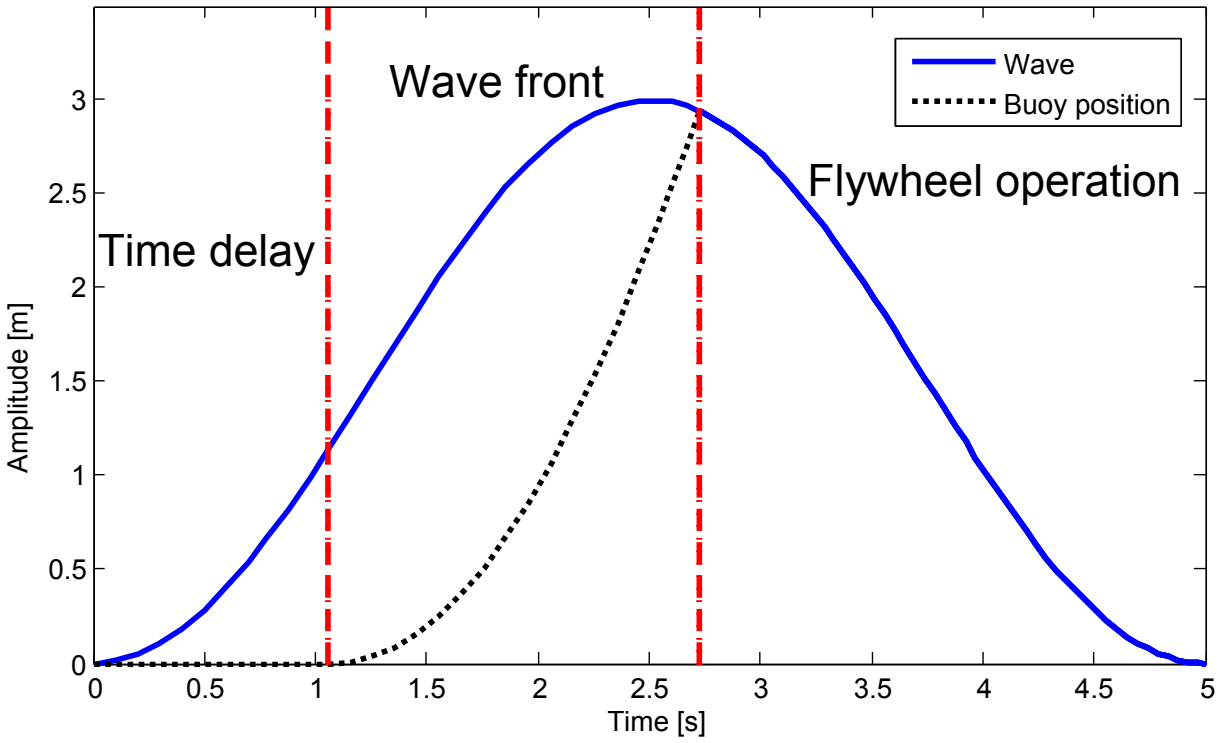

Figure 4.1: Schematic figure of how the control model is divided into three different parts; *time delay*, *wave front* and *flywheel operation*.

4.1 Ideal waves, wave energy and buoy control

Ideal wave data has been created as sinusoidal waves. Varying amplitude (in meters) and length (in seconds) of the waves yields different wave scenarios. Using *MATLAB* as a controller of *Simulink*, key parameters such as amplitude and length of wave, rotational inertia of flywheel, electric torque and delay time, are inserted to a *Simulink* model. The electric torque is the torque in the generator and the delay time is how long the buoy is held still during a wave front. The model simulates how the vertical position of a buoy changes when exposed to an upward lifting force, from the wave, and a downward pulling force, from the flywheel and the generator. The simulation outputs the buoy torque, electric torque, angular velocity of the generator, buoy position, energy uptake from the wave and the mechanical power transmitted to the generator.

The block scheme implementation of the model is divided into two parts, see figure 4.2 and 4.3. The wave front part simulates the behaviour during the rise of the wave and the transfer of energy from the wave front to the flywheel and the generator. The flywheel part simulates the transfer of energy from the flywheel to the generator as no uptake of energy from the wave is made.

4.1.1 The wave front part of the model

The energy supplied in this part comes from the wave front via the freewheel, see figure 2.1. This part starts with a sine wave source, that outputs the vertical position of the surface of the wave, which is compared with the vertical position of the buoy to get how deep the buoy lies in the water, see the *Lifting torque* block in figure 4.2. If the buoy is not fully submerged the depth is d_{over} and if it is fully submerged or more the depth is d_{under}. The two different cases are explained in section 2.3.1. Two expressions, (4.1) and (4.2), are used to convert d_{over} and d_{under} to the lifting forces F_{over} and F_{under} respectively, which are the same as (2.1) and (2.2).

$$F_{over} = ((h_{buoy} - d_{over})\pi\rho_{water}r_{buoy}^2 - m_{buoy})g \tag{4.1}$$

$$F_{under} = (h_{buoy}\pi\rho_{water}r_{buoy}^2(\frac{d_{under}}{h_2} + 1) - m_{buoy})g \tag{4.2}$$

F_{over} and F_{under} are merged together to a common variable F_{buoy}, which is multiplied by r_{fw} to get the developed torque τ_{buoy}, which is the output from the *Lifting torque* block. This torque is controlled by the electric torque τ_e in the generator and the torque exerted by the flywheel $\tau_{fly} = J\partial\omega/\partial t$ to obtain four different control strategies: *constant electric torque*, *constant acceleration*, *constant velocity* and *constant power*; they are all described in more detail in sections 4.2 and 4.3. The *Acceleration torque* block is made according to

$$\tau_{acc} = \tau_{buoy} - \tau_e - \tau_{fly} \tag{4.3}$$

In the *Integrator* block, the resulting lifting force, $F_{buoy} = \tau_{acc}/r_{fw}$, is accelerating the buoy with the acceleration $a_{buoy} = F_{buoy}/m_{buoy}$. The vertical acceleration is integrated to obtain

the vertical velocity, v_{buoy}, of the buoy, and is then integrated again to get the vertical position of the buoy, which is compared with the vertical position of the wave that it all started with. The angular velocity of the freewheel is calculated as $\omega_{fw} = v_{buoy}/r_{fw}$.

During the time that the wave front part of the model is running, i.e. the freewheel is supplying the energy, the total mechanical power, in the *Energy calculator* block, is calculated as

$$P_{mec,tot} = \omega_{fw}(\tau_e + \tau_{fly}) \tag{4.4}$$

which is integrated to get the total energy $E_{mec,tot}$. The power going in to the flywheel and generator is calculated as

$$P_{mec,fly} = \omega_{fw}\tau_{fly} \tag{4.5}$$

$$P_{mec,gen} = \omega_{fw}\tau_e \tag{4.6}$$

which are then integrated respectively to get $E_{mec,fly}$ and $E_{mec,gen}$.

$$E_{mec,tot} = E_{mec,fly} + E_{mec,gen} \tag{4.7}$$

states that the energy going in to the generator and in to the flywheel is the total energy. This model stops when the position of the buoy equals the position of the wave, then the flywheel part starts.

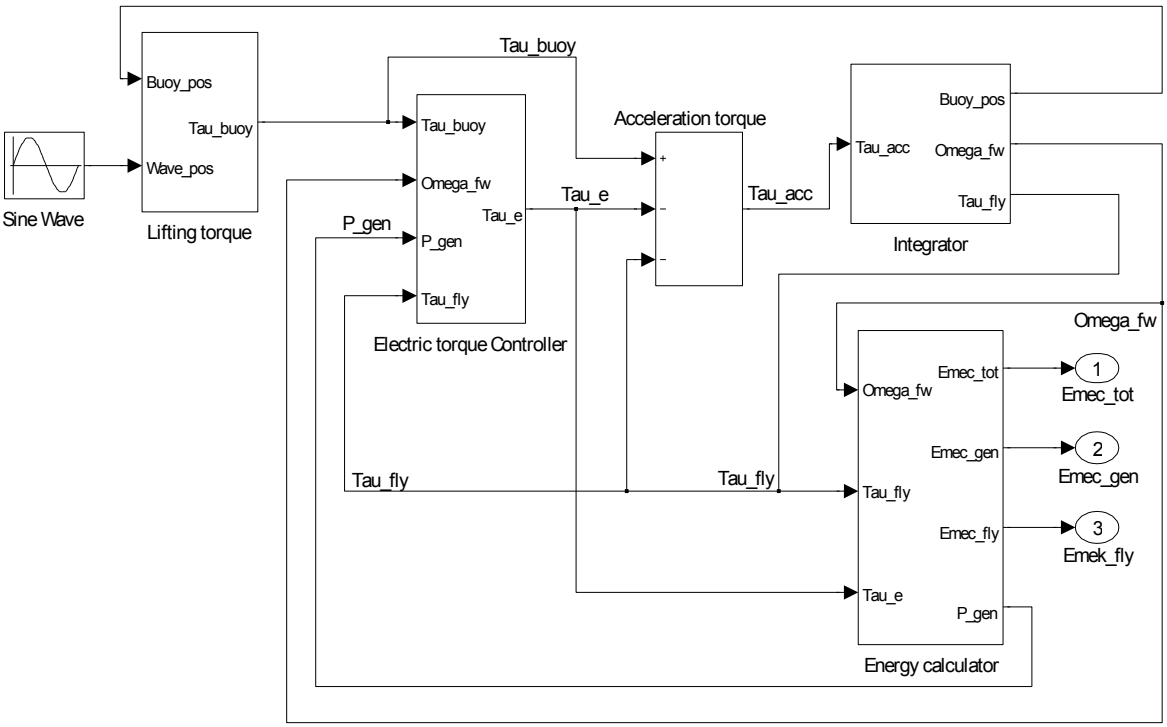

Figure 4.2: The wave front part of the *Simulink* model. The transfer of energy from the wave front to the flywheel and the generator.

4.1.2 The flywheel part of the model

The energy supplied in this part comes from the flywheel. It is the energy that is stored in the flywheel from the wave front part, $E_{mec,fly}$, that is used as the input for the flywheel part, see figure 4.3. In the *Omega converter* block the energy used by the generator, E_{gen}, is subtracted from the starting energy, $E_{mec,fly}$, to get E_{fly}, which is the remaining energy in the flywheel. The angular velocity is then calculated by rewriting (2.11) as

$$\omega_{fly} = \sqrt{\frac{2E_{fly}}{J_{fly}}} \tag{4.8}$$

In order to have a power output until the beginning of the next wave, the electric torque in the generator is controlled by using constant electric torque or constant power control strategies. The constant power and constant electric torque used are shown as τ_{down} and P_{down} in figure 4.3. Either way is a power output calculated that gives a positive $P_{mec,gen}$ until the start of the next wave period. The power in to the generator is calculated as $P_{mec,gen} = \tau_e \omega$, which is then integrated to get $E_{mec,gen}$. $E_{mec,gen}$ should be the same as the constant $E_{mec,fly}$ at the end of the wave period, which is the end of the flywheel part model.

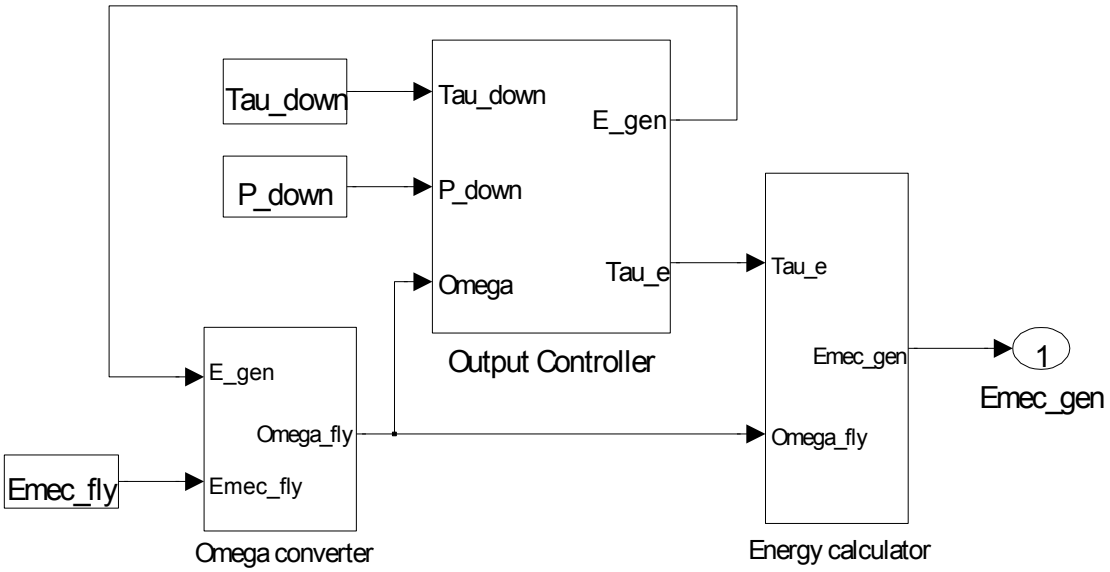

Figure 4.3: The flywheel part of the *Simulink* model. The simulation of the transfer of energy from the flywheel to the generator.

4.2 Analysis of control strategies during wave front operation

The electric torque, τ_e, in the generator can be controlled in several ways, here is τ_e changed according to one of the four control strategies: *constant electric torque*, *constant acceleration*, *constant velocity* or *constant power*. Additionally, τ_e is divided into three different operational parts regardless of the just mentioned control strategies; first is a time delay applied by setting τ_e equal to the lifting force, τ_{buoy}, so that the buoy is at a standstill during the beginning of the wave front; secondly, a τ_e is applied that controls the buoy during its ascent according to one of the four control strategies; at last a τ_e is applied that controls the withdrawal of energy from the flywheel according to the *constant electric torque* or *constant power* control strategies. The concept of applying a delay is meaningful since the energy uptake becomes greater than without a delay. Figures 4.4 to 4.11 shows the results from simulations with a 3 meters high and 5 seconds long wave and a rotational inertia of the flywheel, J_{fly}, of 3000 kgm^2.

All four control strategies are swept in order to find the highest energy uptake that can be achieved from a wave front. The energy uptakes are quite similar to each other but have some differences that distinguishes them from each other.

4.2.1 Constant electric torque

With regards to the wave shape and the rotational inertia of the rotor, the constant electric torque, τ_e, that gives the most energy, is found by sweeping τ_e. The most energy implies the highest energy uptake that can be achieved with a constant τ_e. In figure 4.4, the delay is seen during the first second of the period, the same time that τ_e equals the buoy torque, τ_{buoy}, in figure 4.5. The wave front control strategy with a constant τ_e is fulfilled after the delay, as the constant dashed line in figure 4.5. Due to the keeping of τ_e constant the angular velocity of the rotor, ω, must increase. Thus energy is stored in the rotational inertia of the rotor and flywheel. N.B. that figure 4.5 only shows τ and ω during a wave front, i.e. until the buoy reaches the surface at approximately $t = 2.7$ s. After this, one of the flywheel control strategies is applied, see figure 4.1.

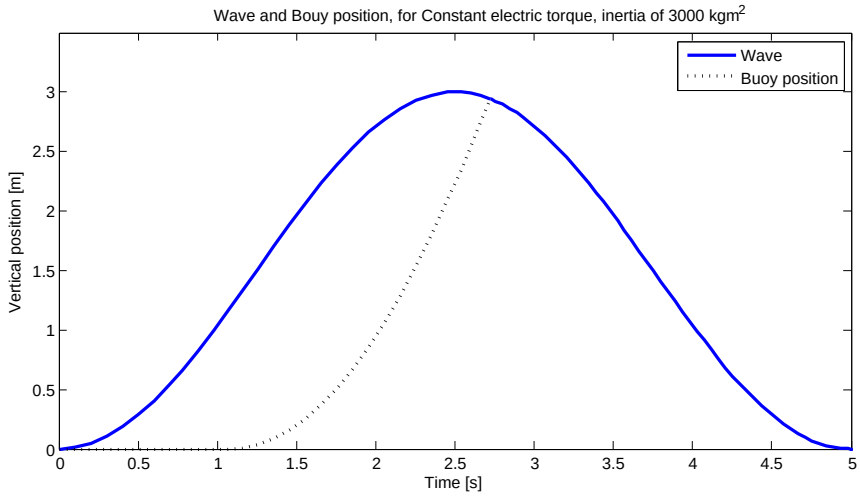

Figure 4.4: Constant electric torque control strategy. The position of the buoy relative to the surface of the wave. Energy uptake is 126.4 kJ from the wave front.

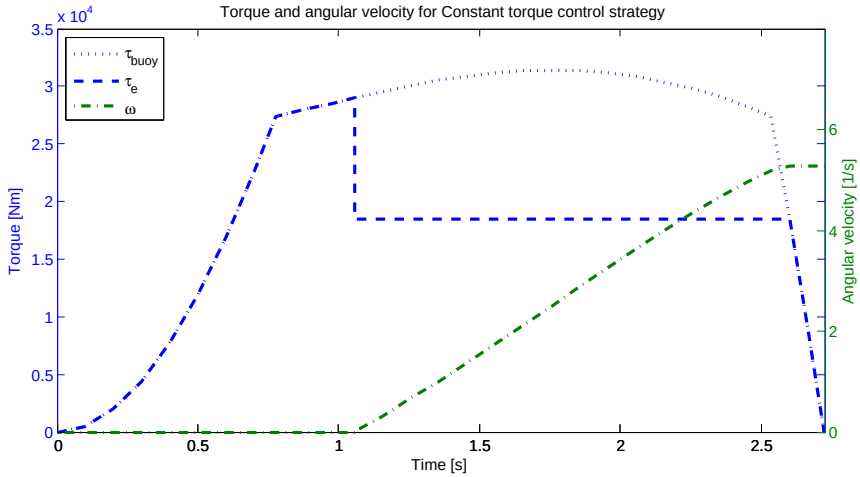

Figure 4.5: Constant electric torque control strategy. After the time delay τ_e is seen to be constant as ω increases with an almost constant acceleration.

4.2.2 Constant acceleration

By keeping the acceleration torque τ_{acc} constant, a constant acceleration can be obtained, see the constant increase in ω in figure 4.7. This differs from the previous control strategy where the electric torque was constant, compare τ_e in figures 4.5 and 4.7. τ_{acc} for the highest energy uptake is found by sweeping τ_{acc} in the same way as τ_e for the previous control

strategy. The electric torque for the constant acceleration control strategy is calculated as

$$\tau_e = \tau_{buoy} - J\frac{\partial \omega}{\partial t} - \tau_{acc} = \tau_{buoy} - \tau_{fly} - \tau_{acc} \tag{4.9}$$

in which τ_{acc} is constant. The flywheel torque also becomes constant since $\tau_{fly} = J\alpha$, where the acceleration term α is constant. After the delay time in figure 4.7, the difference between τ_{buoy} and τ_e is seen to be constant as long as the acceleration is constant, i.e. as long as ω increases at a constant pace.

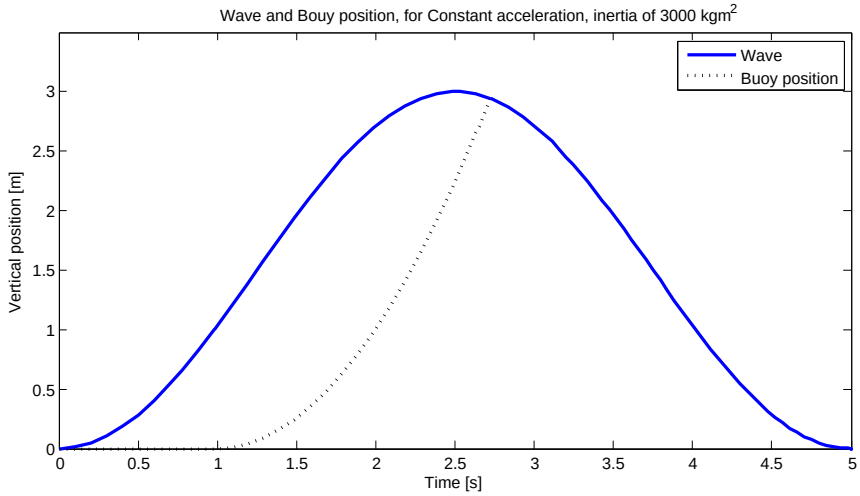

Figure 4.6: Constant acceleration control strategy. The rise of the buoy is smoother than in the previous case. Energy uptake of 125.4 kJ from the wave front.

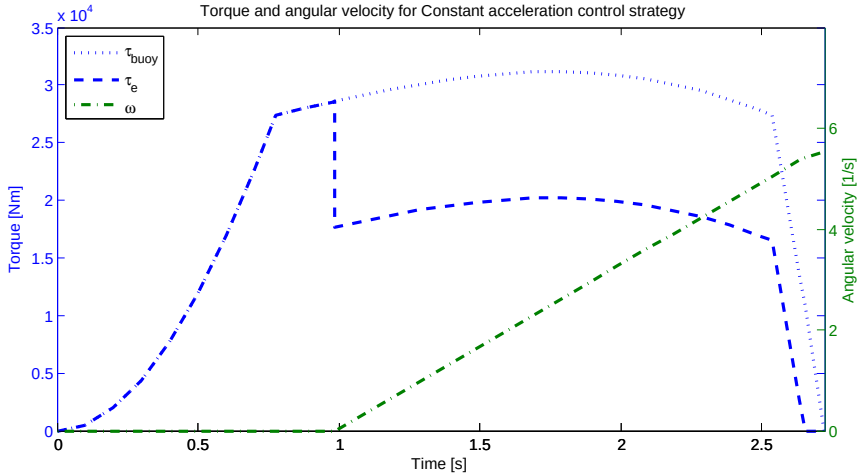

Figure 4.7: Constant acceleration control strategy. After the time delay, τ_{acc} is seen to be constant (the distance between τ_{buoy} and τ_e) and ω increases with a constant acceleration (which can be compared to the previous case of almost constant acceleration).

4.2.3 Constant velocity

During this control strategy, the angular velocity of the freewheel is swept instead of sweeping the torque as in the previous cases. The sweeping process stops when the highest $E_{mec,tot}$ is found. The electric torque is controlled according to the following criteria:

$$\tau_e = \begin{cases} \tau_{buoy} & \text{during the time delay} \\ 0 & \text{during acceleration} \\ \tau_{buoy} & \text{when } \omega \text{ is constant} \end{cases} \tag{4.10}$$

With this control strategy the highest energy uptake obtained is 128.5 kJ. However, figure 4.9 shows that with the current definition of the constant velocity control strategy, power is only developed after the velocity has reached its constant value.

The reason for this control strategy developing the highest energy uptake is probably due to the long delay and the fast reached constant velocity that is withheld during the peak of the wave. Large variations in τ_e makes it more difficult to design a suitable generator, this since the maximum electric torque in a generator is proportional to its size due to that the current is approximately proportional to the torque. Designing a generator for a large variation in τ_e gives a lower utilization rate of the copper compared to if the variations in τ_e were small.

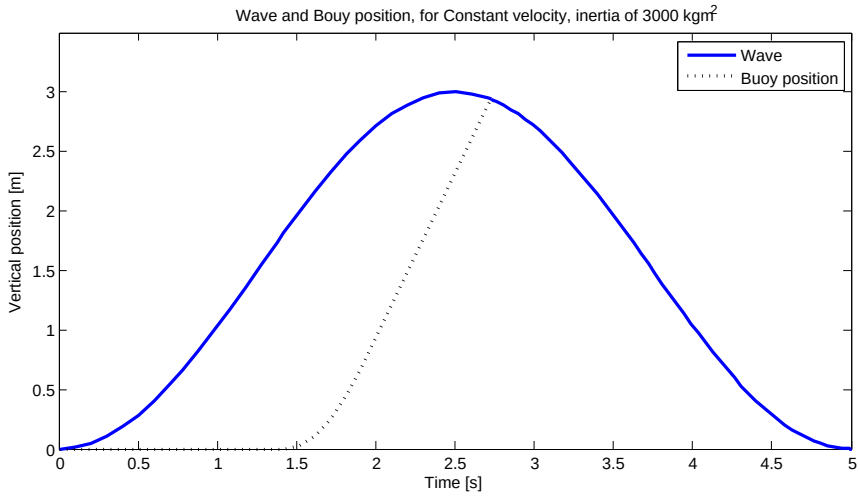

Figure 4.8: Constant velocity control strategy. The rise of the buoy is made at a constant velocity after a short acceleration; compare the straight line of the buoy's position with the previous two. Energy uptake is 128.5 kJ from the wave front.

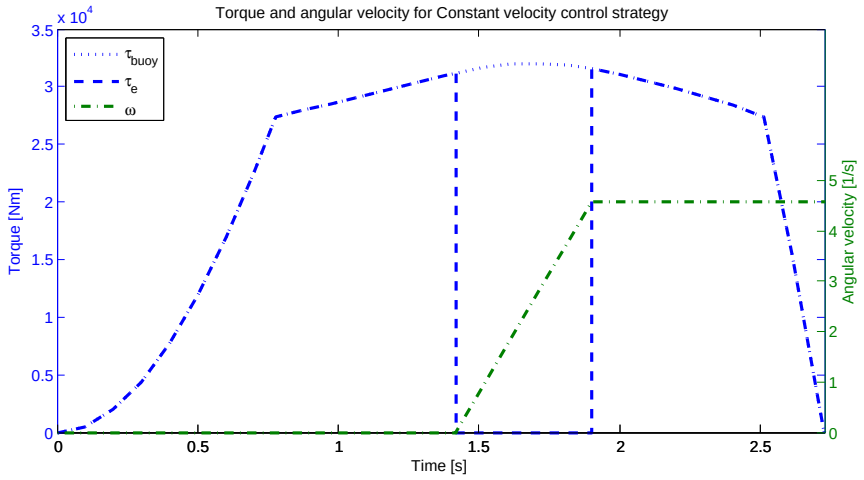

Figure 4.9: The constant velocity control strategy differs quite much from the previous two strategies. After the time delay is a maximum acceleration had with $\tau_e = 0$ followed by a constant ω where $\tau_e = \tau_{buoy}$.

4.2.4 Constant power

To achieve a constant power during the wave front, a starting electric torque is swept as for the constant electric torque control strategy. Figure 4.11 shows how the electric torque is successively reduced in steps as the angular velocity continues to increase when the desired power is met, thus obtaining a fairly constant power, $P = \tau_e \omega$. This gives the smallest energy uptake of 123.3 kJ. A fairly constant power output to the generator should result in a smooth electric output from the generator. The generator has no problem with ω going up and down since this will just make an electric output with different frequencies and voltages that depends on the current ω. As already mentioned in the previous case, large variations in τ_e make it more difficult to design a suitable generator.

The small variations in power in figure 4.11 that makes the power fairly constant instead of constant is due to the control strategy used. When no information of the energy uptake can be had beforehand there is no way to know how big the overshoot in power compared to the desired constant power will be. One way to control the power to be fairly constant is then to decrease the electric torque by one step whenever reaching the desired power.

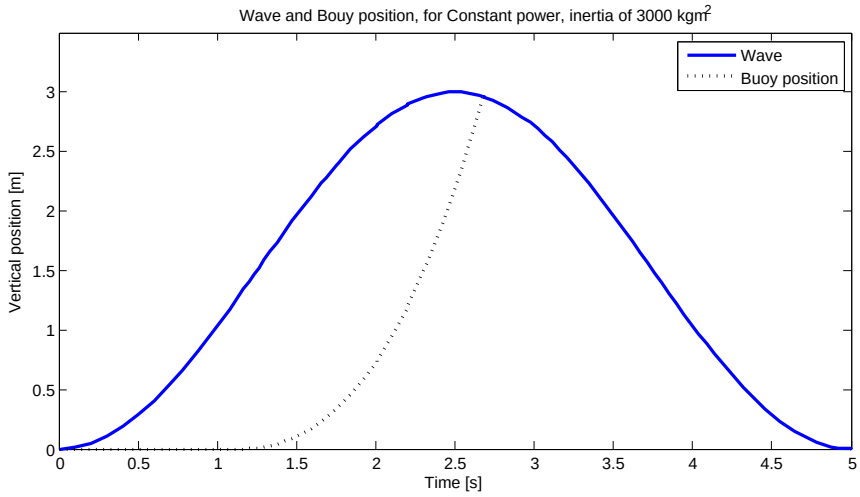

Figure 4.10: Constant power control strategy. Here is the rise of the buoy similar to the first two strategies. Energy uptake of 123.3 kJ from the wave front.

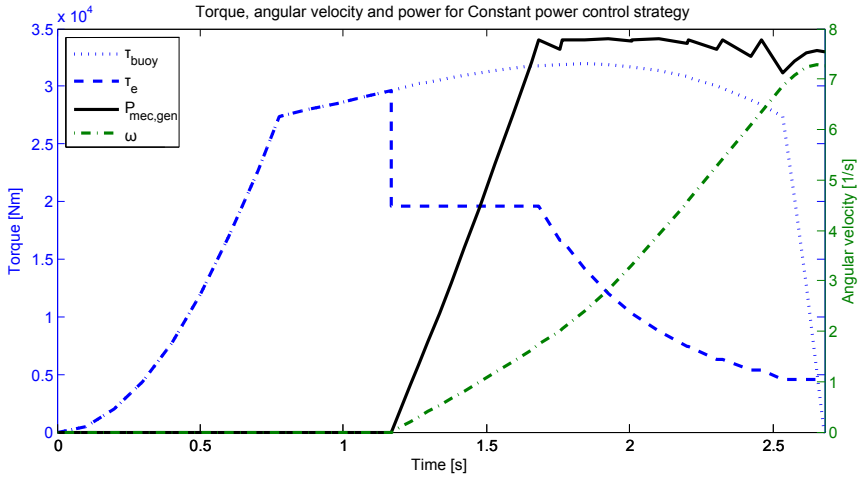

Figure 4.11: The constant power control strategy is the same as the constant electric torque control strategy until the desired power is met. Then is a fairly constant power obtained by reducing τ_e in steps as ω increases.

4.3 Analysis of control strategies during flywheel operation

After the buoy has reached the surface of the wave, the flywheel control part of the torque τ_e begins and the freewheel no longer drives the axis. The energy that is stored in the flywheel is independent on which control strategy that was used during the wave front, except for which J_{fly} that was chosen and at which time the flywheel operation begins. However, the energy is withdrawn by either keeping the electric torque constant or the

power withdrawal constant. Figures 4.12 and 4.13 were generated with a 3 meters high and 5 seconds long simulated wave and a rotational inertia of the flywheel of 4500 kgm^2.

4.3.1 Constant electric torque

During the flywheel part of the model a constant electric torque is calculated, which makes it possible to transfer all the stored energy in the flywheel to the generator before the start of the next wave front. This is done according to

$$\tau_e = \tau_{down} = J\frac{\partial \omega}{\partial t} = J\frac{\omega_{fly}}{t_{stop} - t_{break}} \tag{4.11}$$

where t_{stop} is the stop time for the flywheel model, t_{break} is the time at which the wave front part model stops, τ_{down} is the constant electric torque during the flywheel operation and ω_{fly} is the angular velocity at the start of the flywheel part, see (4.8). Keeping τ_e constant during the withdrawal of energy results in a linear power and angular velocity decrease, see figure 4.12 after the vertical dotted line. The keeping of τ_e constant during both wave front and flywheel operation results in small variations in torque after the time delay part has been cleared. Small variations in torque is important if one wants to design a generator for a small current interval, this since current is approximately proportional to torque as mentioned in section 4.2.3.

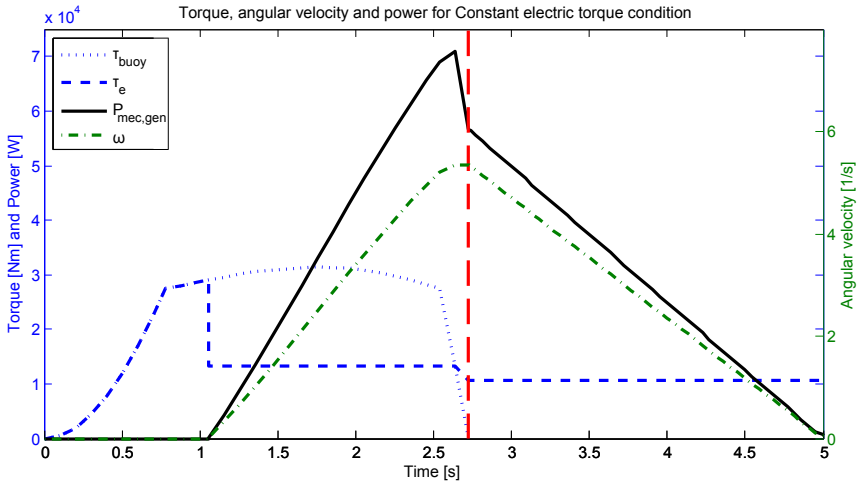

Figure 4.12: Constant electric torque control strategy during both wave front and flywheel operation (before and after the vertical dotted line), with an inertia of 4500 kgm^2.

4.3.2 Constant power

During the flywheel operation, the power is kept constant by extracting the same amount of power, P_{down}, from the flywheel to the generator until the start of the next wave period.

A corresponding electric torque is calculated with (4.12), see figure 4.13 after the vertical dotted line.

$$\tau_e = \tau_{fly} = \frac{P_{down}}{\omega_{fly}} = \frac{E_{mec,fly}}{\omega_{fly}(t_{stop} - t_{break})} \tag{4.12}$$

where ω_{fly} is the same as in (4.8). For the product $\tau_e\omega$ to become constant when ω both increase and decrease during the whole wave period, τ_e is controlled to vary inversely proportional to ω, which is seen in figure 4.13. The fairly constant power had during the wave front is explained in section 4.2.4. The constant power control strategy generate very large electric torque variations, which is an unwanted property when designing a generator, as explained in section 4.2.3. The torque τ_e can be limited to a certain maximum torque, but that will result in a slight power decrease at the end of the period.

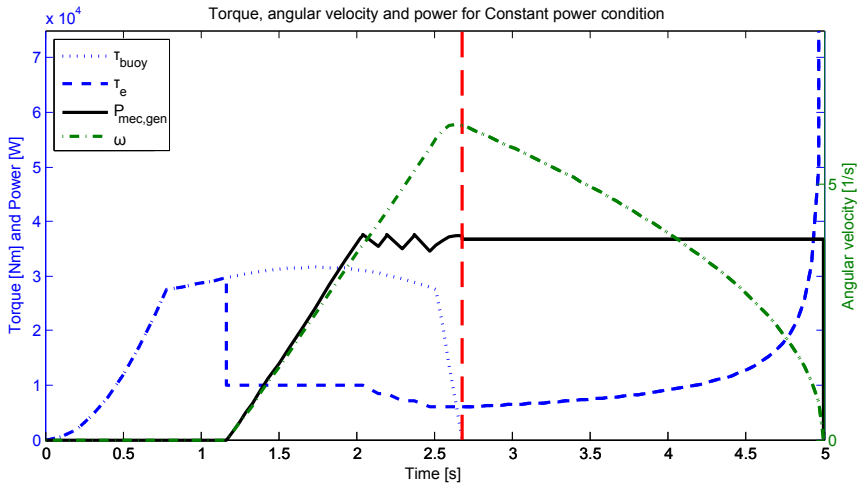

Figure 4.13: Constant power control strategy during both wave front and flywheel operation (before and after the vertical dotted line), with an inertia of 4500 kgm^2.

4.4 Dimensioning the electric torque

Constant electric torque with and without a rotational inertia of the flywheel, J_{fly}, and constant power with J_{fly} are the three cases that have been chosen for the dimensioning. The case without J_{fly} were chosen to be able to compare the difference in power and electric torque that could be had when using J_{fly}. The constant electric torque and constant power control strategies were chosen since these were considered as the most suitable and promising strategies. Each have been regulated for the uptake of most energy at the same time as following its control strategy. They have also been regulated to keep as constant τ_e and as low maximum τ_e as possible. The maximum electric torques $\tau_{e,max}$ will later be used to dimension the size of three corresponding generator designs.

During the simulations it was found that all cases have almost the same energy uptake, from the wave front, with an average of 123.5 kJ. The delay time in the constant electric torque cases is 1.06 s and in the constant power case 1.17 s.

In figures 4.14 to 4.16 the maximum electric torque that the generator needs to exert can be seen. Even though the scaling is different in figures 4.14 to 4.16 it can be seen that the buoy torque has the same shape and size regardless of which case; this is because the energy uptake is approximately the same for all three cases.

The time delay applies here as well, but not with the rotor at standstill as in sections 4.2 and 4.3. Instead the electric torque is somewhat smaller than the buoy torque. This allows for an increase in the angular velocity and developed power earlier than before, resulting in an overall less steep power profile, since power is developed during a longer period of time. E.g. compare figures 4.5 and 4.15, with a constant electric torque control strategy with a change in J_{fly} from 3000 to 6500 kgm^2 and the change from a stationary rotor to a rotating rotor during the time delay.

4.4.1 Case 1: Constant electric torque without flywheel

For the constant electric torque and no J_{fly} case τ_e is not entirely constant after the time delay at 1.06 s, see figure 4.14. This is because the torque (τ_e) that gives the most energy is used. Instead, the behaviour of τ_e is similar to the τ_e achieved with a constant acceleration control strategy (see section 4.2.2), which means that more energy is extracted with this control strategy than with constant electric torque when not keeping the rotor at standstill during the time delay.

Since this case have no J_{fly}, only the wave front part is shown in figure 4.14, i.e. no energy is stored in the flywheel since there is no flywheel and thus no energy can be transferred to the generator during the flywheel operation part of the model. Thus, all power is developed during the wave front resulting in a large power peak, which the generator needs to take care of as efficiently as possible.

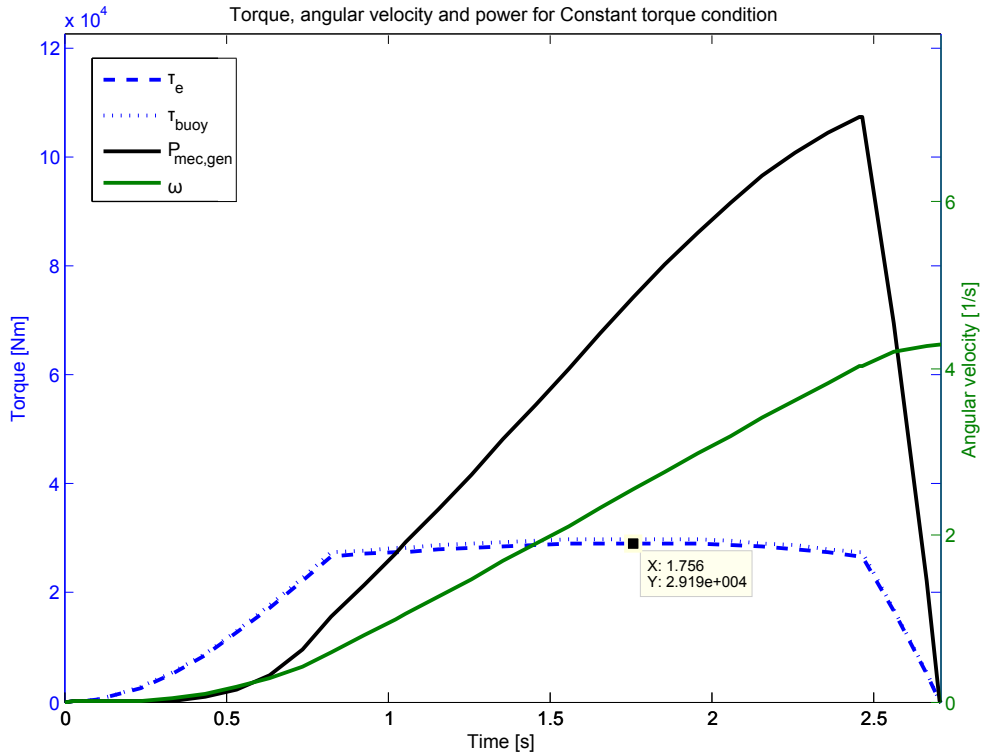

Figure 4.14: Constant electric torque control strategy with no rotational inertia. The time delay is 1.06 s and the energy uptake during the wave front is 123.53 skJ.

The two control strategies with J_{fly} generate similar maximum electric torques. The constant electric torque control strategy with $J_{fly} = 6500$ kgm^2 gets a maximum of $\tau_{e,max} = 14.97$ kNm and the constant power control strategy with $J_{fly} = 7500$ kgm^2 gets a maximum of $\tau_{e,max} = 13.48$ kNm.

4.4.2 Case 2: Constant electric torque with flywheel

The constant electric torque with a rotational inertia of 6500 kgm^2 has, as in the previous case, also a τ_e that is not entirely constant after the time delay at 1.06 s. This is due to the same cause as previously mentioned. During the time delay, the electric torque in the generator is less than in the case without J_{fly}, this since the flywheel stores some of the torque exerted by the buoy as energy. This energy is withdrawn with a constant τ_e during the flywheel part of the model, see figure 4.15 from 2.7 s and forth. The difference between figures 4.14 and 4.15 shows clearly how the same control strategy can be better utilised with a flywheel. Due to the keeping of τ_e constant, the power is increasing with the increase of ω and, after reaching its peak value, decreasing with the decrease of ω.

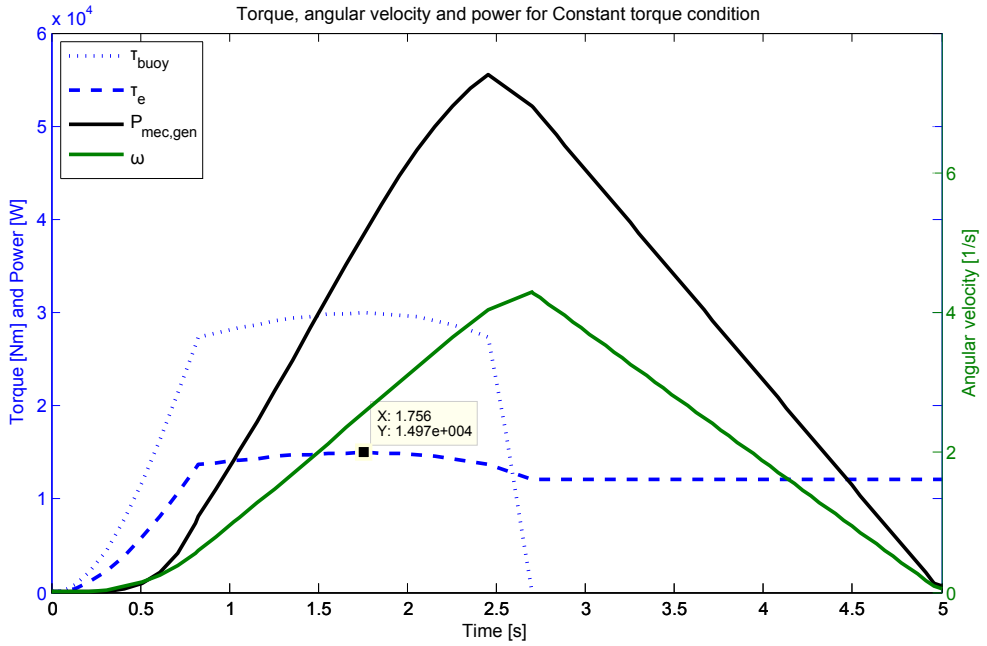

Figure 4.15: Constant electric torque control strategy with a rotational inertia of 6500 kgm^2. The time delay is 1.06 s and the energy uptake during the wave front is 123.49 kJ.

4.4.3 Case 3: Constant power with flywheel

With a J_{fly} of 7500 kgm^2 the constant power control strategy has the largest rotational inertia of the three cases. From a generator design perspective this is the most promising case since it has a fairly constant power profile with no separate peaks and the lowest $\tau_{e,max}$ needed. Still, it has the same energy uptake as the previous two cases. During the time delay, until 1.17 s, τ_e is even smaller than in the case of constant electric torque with J_{fly}. This since the rotational inertia is greater than before. After 1.17 s, τ_e is constant until the (predefined) desired power is reached. The power is kept fairly constant by reducing τ_e in steps until the wave front is over at approximately 2.7 s. Then, during the flywheel operation τ_e is steadily increased, as ω is decreasing, until τ_e reaches $\tau_{e,max}$ and is kept constant at the maximum allowed electric torque. As τ_e reaches its maximum and ω continues to decrease, the power starts to decline. The power and the angular velocity reach zero at the end of the wave period.

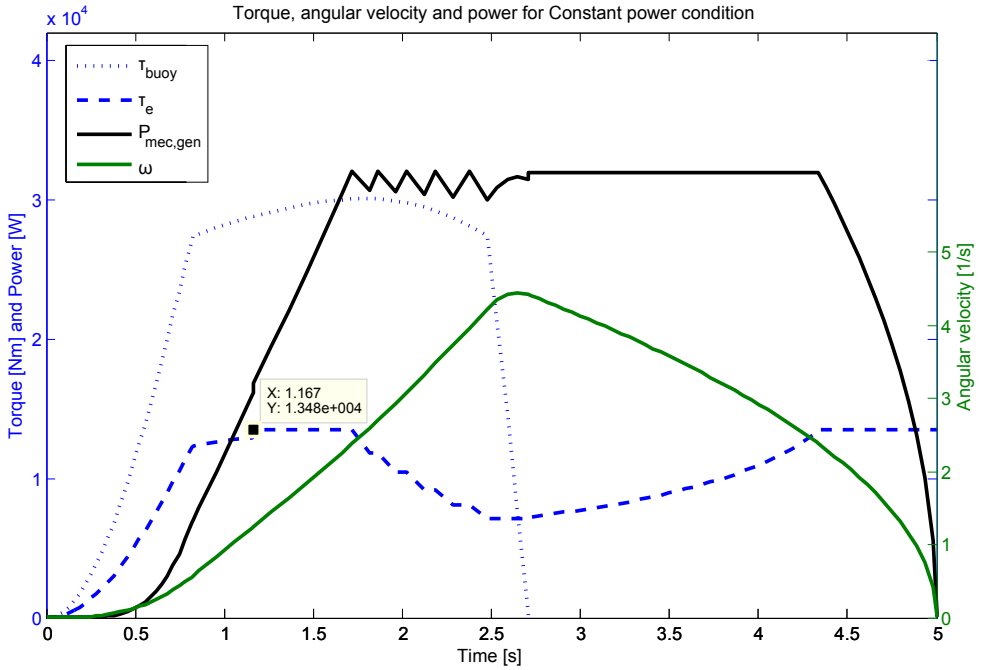

Figure 4.16: Constant power control strategy with a rotational inertia of 7500 kgm^2. The time delay is 1.17 s and the energy uptake during the wave front is 123.55 kJ.

Summing up From this section, three generator designs can be made. If utilising a gear box with an exchange ratio of $G = 10$ these three designs have the requirements seen in table I.

TABLE I: The requirements for the three generator designs with $G = 10$.

	Constant τ_e with $J_{fly} = 0$ kgm^2	Constant τ_e with $J_{fly} = 6500$ kgm^2	Constant $P_{mec,gen}$ with $J_{fly} = 7500$ kgm^2
Max electric torque [Nm]	2919	1497	1348
Max angular velocity [rpm]	409	410	422

5 Generator design

In order to make the three generator designs, a first PMSG design was made with the help of the analytical design tool *RMxprt*, see figure 5.1. See chapter 3.1 for the corresponding names of the different parts of the generator design. The number of slots and poles were decided together with the air gap length and the maximum flux density. A stator diameter was set and the remaining design parameters were swept in *RMxprt* according to the decided number of slots and poles, air gap length and maximum flux density. The design made in *RMxprt* was then exported to the finite element analysis (FEA) tool *Maxwell*. There, the design was scaled according to the three cases previously presented, using a maximum current density of 5 A/mm^2 together with the corresponding maximum electric torque as design criteria.

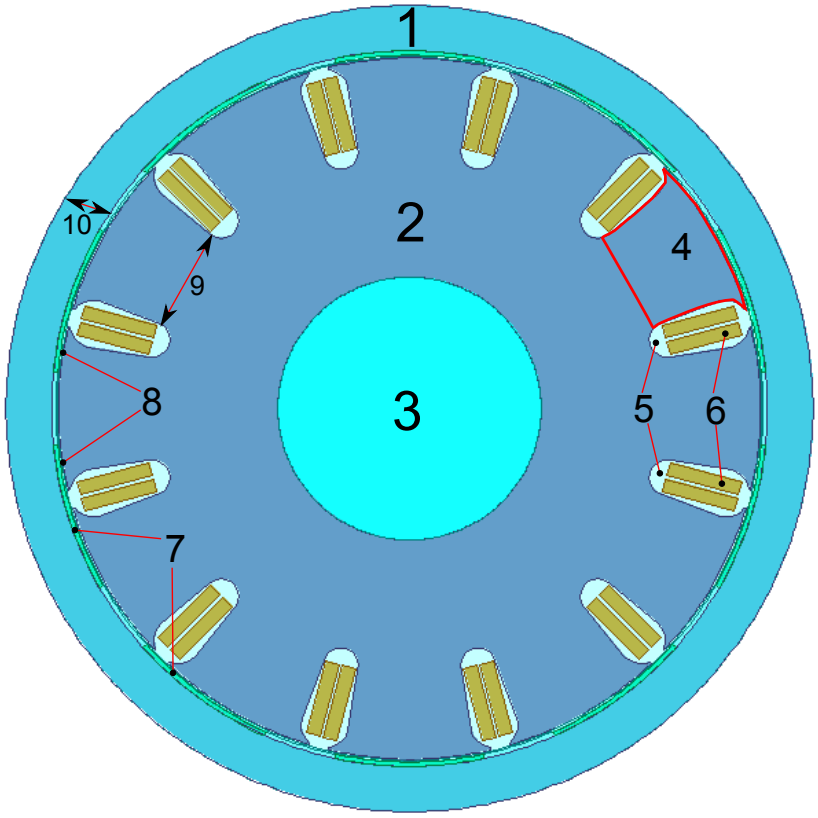

Figure 5.1: Cross-section of the generator design. See chapter 3.1 for the corresponding names of the different parts of the generator design.

The diameter of the stator was arbitrarily chosen to 400 mm and since the electric torque is approximately linearly proportional to the length of a generator, the length of the design was chosen to 1000 mm. Thus could the maximum electric torque easily be altered by scaling the design.

The generator design is made as an exterior rotor machine since this gives the rotor a larger rotational inertia, J_{rot}, than if an internal rotor configuration would have been used. At first, the rotor was made quite large, to simulate a flywheel with a couple of thousand kgm^2, but later it was reduced to the minimum size needed of about 3 to 14 kgm^2 according to the maximum flux density allowed in the rotor yoke for respective design, see section 5.2. J_{rot} were then compared with the rotational inertia of the flywheel, J_{fly}, to see how big a part J_{rot} were of J_{fly} and thus see if J_{rot} have any effect on J_{fly} and the total rotational inertia of the system.

5.1 Slots and poles

The generator has been designed with 12 slots and 5 pole-pairs as an exterior rotor machine, see figure 5.1. The number of slots and poles were arbitrarily decided by discussion and comparison with a similar design [12]. Through reiteration of the design, the number of slots and poles would probably have been changed, but the goal with this thesis is the comparison between the three different designs (cases) and not an optimized generator design.

The frequency f of the electric output is dependent on both the number of pole-pairs p and the synchronous speed N_s of the rotor as in (5.1).

$$f = \frac{N_s \cdot p}{60} \tag{5.1}$$

This suggests that if a higher frequency output is wanted, either the pole-pair number can be increased by adding more permanent magnets or the synchronous speed of the rotor can be increased by utilising a higher exchange ratio than $G = 10$.

5.2 Air gap and magnetic flux density

The air gap length was set to 1.5 mm since a longer gap would have increased the reluctance of the air gap and thus the total reluctance of the magnetic circuit. The total reluctance is always tried to be kept as low as possible to minimize losses. A shorter air gap would have been too small of a margin between the stator and rotor from a mechanical point of view. The mechanical limits are e.g. glitches in the bearings and thermal expansion of the rotor and stator during operation.

The thickness of the permanent magnets were set to be 2.5 mm by sweeping different thicknesses according to the criteria of $B < 1.2$ T. In (5.2), which is (3.7) with (3.8) and (3.9) inserted, we assume that the air gap area and the magnet area are the same, $A_g = A_m$, i.e. the flux linkage moves straight through the air gap. This makes the flux linkage in the magnet, Φ_m, independent of the diameter of the machine. Thus, Φ_m will only be dependent

on the thickness of the magnet L_m and the length of the air gap L_g.

$$\Phi_m = \frac{1}{1 + f_{LKG}\left(\frac{\mu_0 \mu_{rec} A_m}{L_m} \cdot \frac{L_g}{\mu_0 A_g}\right)} \Phi_r = \frac{1}{1 + f_{LKG}\left(\frac{\mu_{rec} L_g}{L_m}\right)} \Phi_r \tag{5.2}$$

Since we know that $\Phi_m = A_m B_m$ and $\Phi_r = A_m B_r$ we can rewrite (5.2) as

$$B_m = \frac{1}{1 + f_{LKG}\left(\frac{\mu_{rec} L_g}{L_m}\right)} B_r \tag{5.3}$$

By keeping L_g and L_m constant, the flux density in the magnet, B_m, will thus be constant even when scaling the generator design. The flux density in the air gap will also be constant if $\Phi_g = \Phi_m$ is assumed, i.e. that all the flux that flows in the magnet flows through the air gap, since $A_g = A_m$ was assumed. Due to the approximations made, the magnetic flux density will not be entirely constant when scaling the generator design, but sufficiently constant to fulfil the design criteria.

In addition to the design criteria of $B < 1.2$ T, the magnet thickness was also swept in order to optimize the design for efficiency. Most of the design parameters were swept according to these two design criteria. The 1.2 T value were arbitrarily chosen so that magnetic saturation of the core should not occur during high power operation.

In order to have roughly the same magnetic flux density inside the teeth and the rotor yoke the width of the stator teeth is about twice the size of the thickness of the rotor yoke. This since the magnetic flux, Φ, flowing out from the stator teeth splits into two fluxes which goes its respective ways in the rotor yoke, i.e. one to the left and one to the right with respect to Φ's previous direction, see figure 5.2.

Since the diameter of the stator was set to 400 mm and the design criteria of $B < 1.2$ T was chosen, the diameter of the rotor was hence set to 460 mm.

As shown in section 3.1.2 the induced magnetic flux, Φ_I, is inversely proportional to the total reluctance, $\mathcal{R}$, according to

$$\Phi_I = \frac{NI}{\mathcal{R}} \tag{5.4}$$

$\mathcal{R}$ in the magnetic circuit is the sum of the reluctance in the air gap and in the iron guide

$$\mathcal{R} = \mathcal{R}_g + \mathcal{R}_i \tag{5.5}$$

where the air gap reluctance $\mathcal{R}_g$ is one or two orders of magnitude larger than the iron guide reluctance $\mathcal{R}_i$. Since $\mathcal{R}_g >> \mathcal{R}_i$ the total reluctance of the magnetic circuit is kept approximately constant when scaling the generator with a constant air gap and magnet thickness.

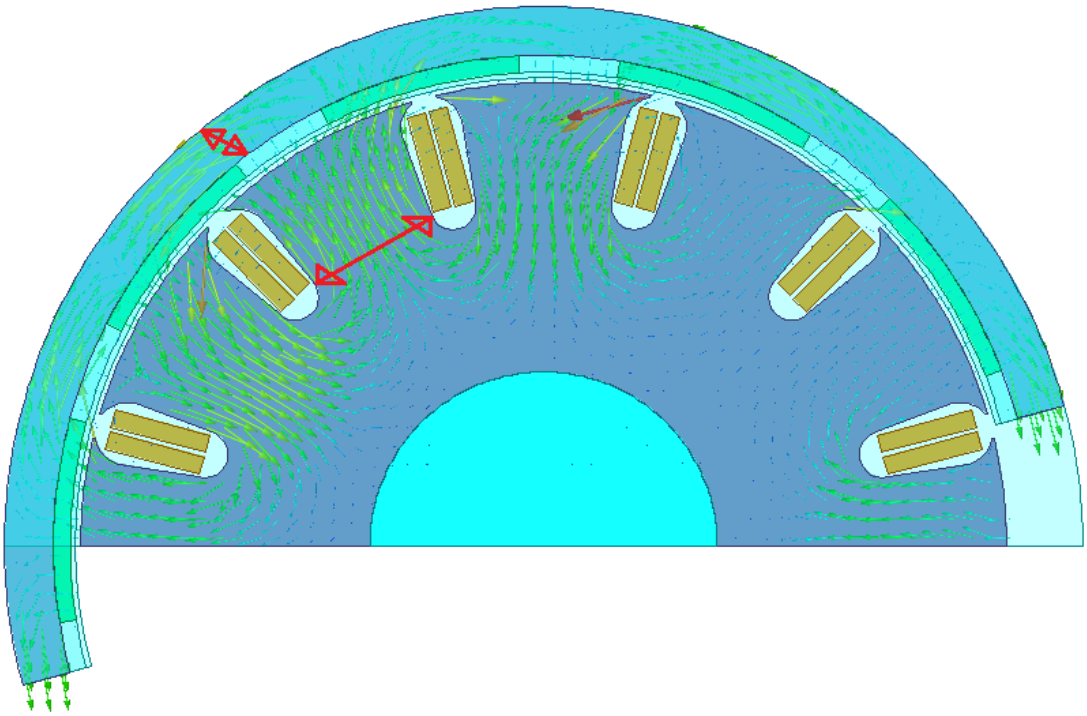

Figure 5.2: Half of the cross-section of the generator design. The distribution of the magnetic flux inside the stator yoke, stator teeth and rotor yoke.

5.3 Flux linkage and induced voltage

A pole embrace of 0.67, i.e. two thirds, is needed in order to get as low harmonic content as possible in the generated flux linkage (see figure 5.3) and induced voltage (see figure 5.5). This to get a smooth torque without ripple while sinusoidal currents are drawn from the generator. The harmonic content of the flux linkage is very low, see figure 5.4, the highest harmonic is the 11th, which is only 0.38% of the fundamental component. The fundamental component, ψ_m, is 1.287 Wb.

The harmonics in the induced voltage is a bit higher, see figure 5.6. The 11th harmonic is still the highest, but is now 4.14% of the fundamental component, which is 403.92 V.

The 90° shift between the flux linkage and the induced voltage is seen by comparing figures 5.3 and 5.5 for a phase.

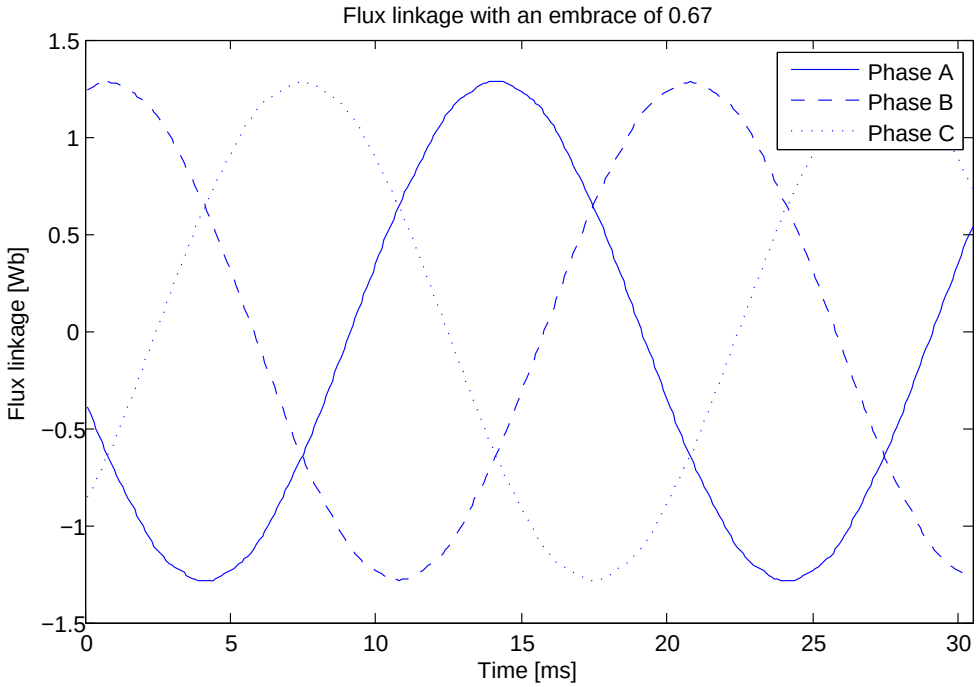

Figure 5.3: The flux linkage in the generator design with a pole embrace of 0.67.

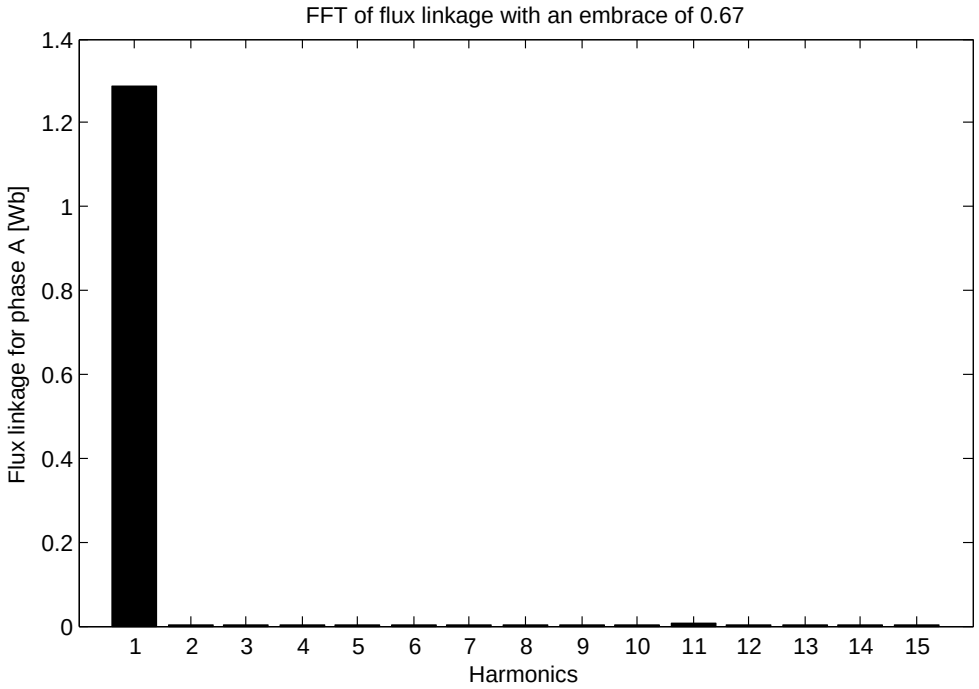

Figure 5.4: FFT of the flux linkage shows low harmonic content.

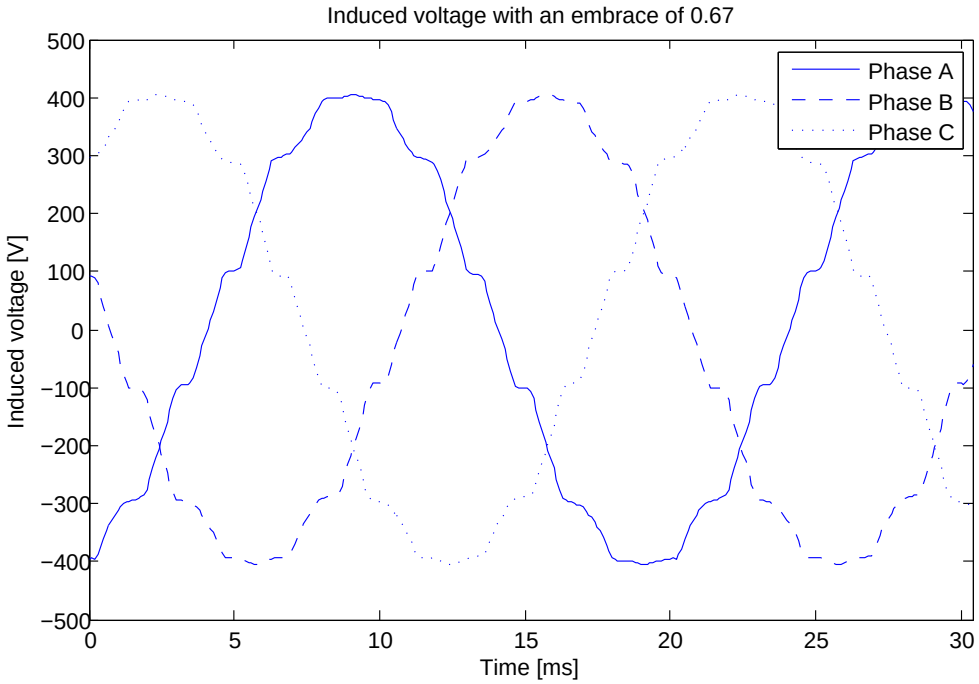

Figure 5.5: The induced voltage in the generator design with a pole embrace of 0.67.

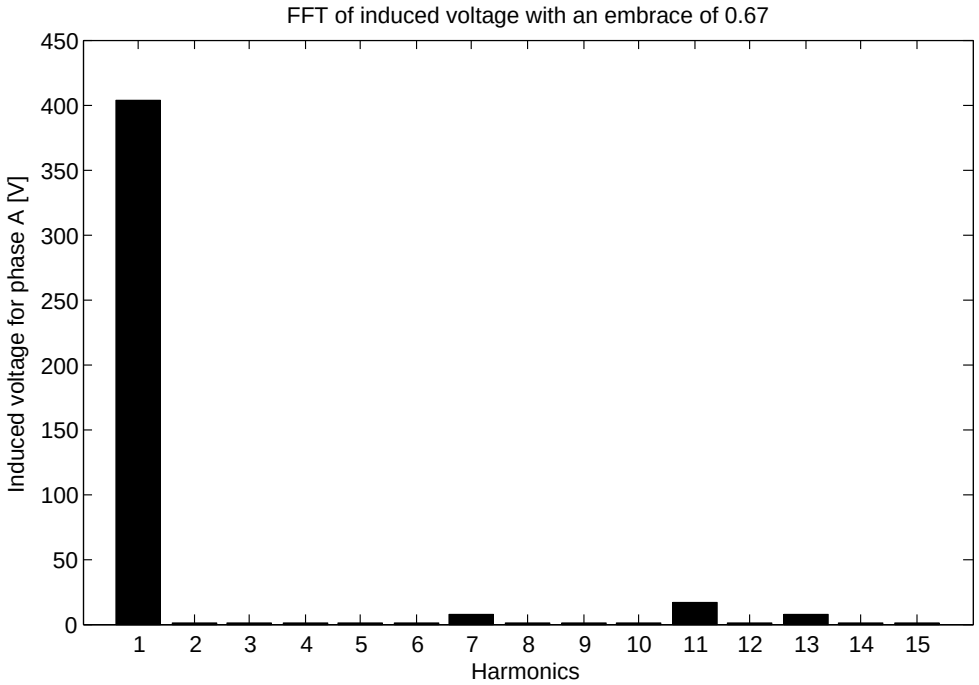

Figure 5.6: FFT of the induced voltage showing the harmonic content in the higher harmonics (7th, 11th and 13th).

5.4 Size of generator

The dimensioning of the generator design was made according to a set current density giving the phase currents and a set maximum electric torque. Scaling the design with a rms current density of 5 A/mm^2 gave different maximum electric torques depending on the diameter of the scaled generator design. According to reference [10], the typical current density for a totally enclosed machine is between 1.5 and 5 A/mm^2. Even though the size of the generator is not important for the application in this thesis, the highest typical current density was chosen since the generator is designed for the maximum electric torque needed. Thus, an efficient use of the copper is achieved.

According to [10], a common length/diameter ratio for radial flux machines is around 1. In order to get the length l and the diameter d of the design equal a maximum electric torque $\tau_{e,max}$ larger than the ones found for the three cases, in the end of section 4.4, is needed. Utilising the approximation that the maximum electric torque is proportional to the length of the machine, the torque $\tau_{e,max}$ for the 1000 mm design is calculated by

$$\tau_{e,max} = \frac{\tau_{e,max,1}}{l} \tag{5.6}$$

where $\tau_{e,max,1}$ is the maximum electric torque wanted for the $l = d$ design and l is the length where $l = d$ gives the needed $\tau_{e,max}$. Since the maximum electric torque for the $l = d$ design is known, the variable $l = d$ is iterated until the calculated maximum electric torque for the 1000 mm design satisfies Eq. (5.6).

With a decided current density and three maximum electric torques, the scaling of the generator design may begin. Consequently, simulations were performed in the finite element analysis (FEA) program *Maxwell*. Starting with the original design and a few scaled designs it was seen that the largest design needed was the original size. The original design giving about 8000 Nm at a diameter of 460 mm down to a scaling giving about 1000 Nm at a diameter of 140 mm were chosen as the limits of the interval. Approximately 70 simulations were performed in order to obtain the dependency between the outer diameter of the rotor and the maximum electric torque, see figure 5.7. The dimensions of the original design were hence scaled with a factor n, on the interval $0.3 \leq n \leq 1.0$ in 0.01 steps.

Further, with the help of the FEA program *Maxwell*, a transient analysis was performed during one to two electrical periods on each scaling. The simulation needs the currents in each phase as input data. The rms-value of the current, I_{rms}, is calculated as the product between the rms-value of the current density and half the cross sectional area of one coil (half since the same current flows through the coil on both sides of a tooth).

In order to have an electric torque, the currents are set in the q-direction. The direction is found by looking at where, in figure 5.5, the induced voltage in a phase is crossing zero with a positive or negative derivative. Choosing phase A it was seen that the positive q-direction is at 75 electrical degrees or 15 mechanical degrees. One way to set the current is by setting the start position of the rotor to 15° and begin the positive derivative zero crossing of the phase A current here. The phase currents are put out as in a common three phase system with a peak phase current of $\sqrt{2}I_{rms}$.

The 70 simulations shows a close to linear relation between the outer diameter of the rotor and the maximum electric torque in the interval $900 < \tau_{e,max} < 8000$ Nm and $140 < d < 460$ mm in figure 5.7. The simulated points were extrapolated in *MATLAB* to get a higher resolution. This in order to pinpoint the calculated torques and their corresponding outer diameters.

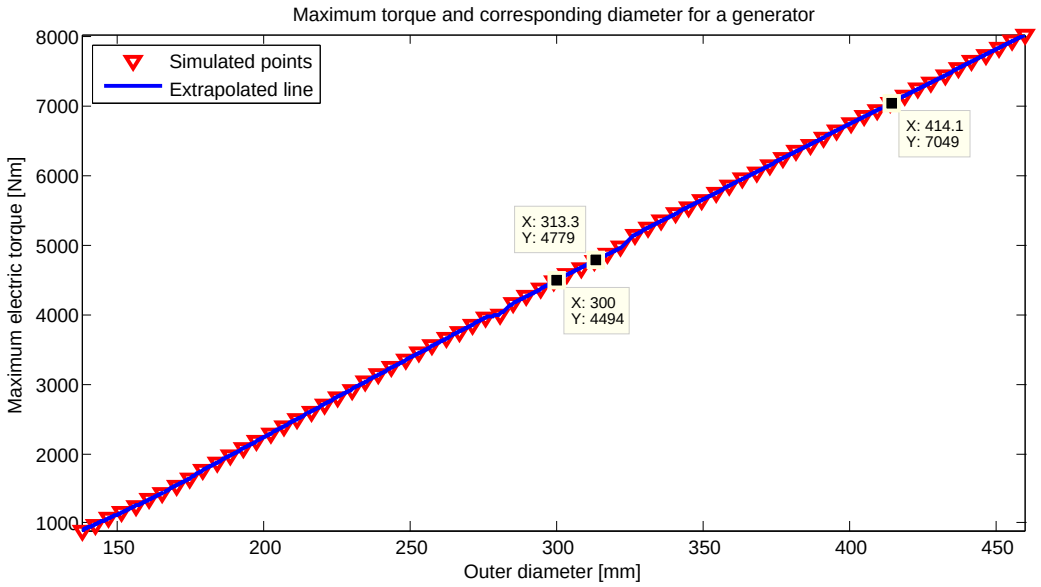

Figure 5.7: The maximum electric torque dependence on the outer diameter of the generator. At an outer diameter of 414.1 mm is case 1 seen, at 313.3 mm case 2 and at 300 mm case 3.

Figure 5.7 shows the $\tau_{e,max}$ achieved with $l = 1000$ mm. The torques ($\tau_{e,max}$) that are used in each of the three cases to get a length/diameter ratio of 1 are shown in the figure as data tips.

A graphical comparison made between the three generator designs is shown in figure 5.8. As the volume between the design without a flywheel and those with a flywheel is more than halved, the material consumption between the first and two other designs is more than halved. This can be seen in table II for copper and iron. The consumption of magnets is not as significant since the same magnet thickness is used in all designs.

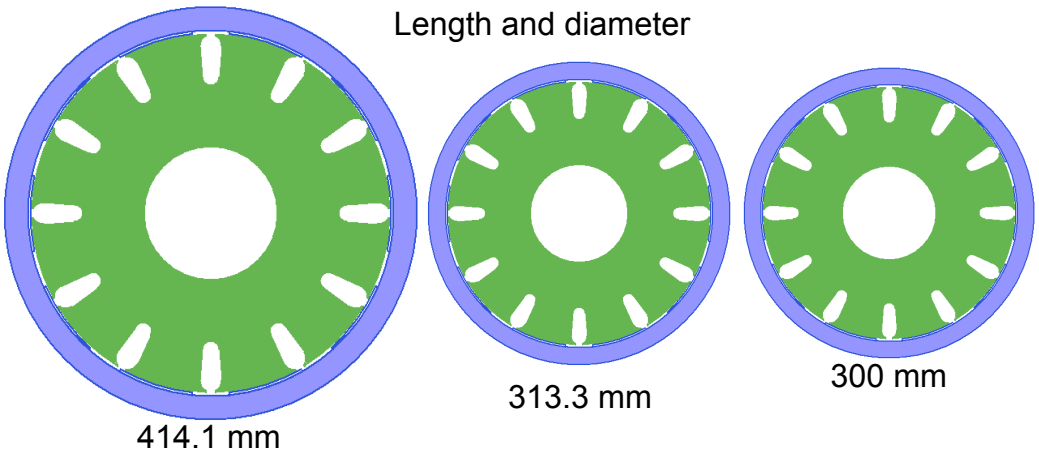

Figure 5.8: Size comparison. Largest outer diameter and length (414.1 mm) to obtain the largest torque (2919 Nm) and smallest outer diameter and length (300 mm) to obtain the lowest torque (1348 Nm).

TABLE II: The material consumption when using a flywheel can be halved compared to when not using a flywheel.

	Constant τ_e with $J_{fly} = 0$ kgm^2	Constant τ_e with $J_{fly} = 6500$ kgm^2	Constant $P_{mec,gen}$ with $J_{fly} = 7500$ kgm^2
Max electric torque [Nm]	2919	1497	1348
Outer diameter [mm]	414.1	313.3	300
Material Consumption:			
Copper [kg]	23.52	10.16	8.89
Magnets [kg]	5.83	3.36	3.08
Iron [kg]	168.90	72.34	63.19
Rotational inertia of rotor, J_{rot}, on both sides of gear box:			
J_{rot} on generator side [kgm^2]	14.3	4.1	3.5
J_{rot} on flywheel side [kgm^2]	1430	410	350

As mentioned in the beginning of this chapter, a comparison was made between the rotational inertia of the rotor and the rotational inertia of the flywheel. The rotational inertia of the rotor is transformed to the flywheel side in order to compare it with the rotational inertia of the flywheel. Having three different rotor diameters that should be compared with three different rotational inertias gives the two last rows in table II. The rotational inertia of the rotor on the flywheel side is the equivalent J_{rot} that would be had if the rotor were on the flywheel side of the gear box, with a gear box ratio of $G = 10$ as mentioned in the end of section 2.3.3. The rotational inertias of the rotor have been calculated according to (2.10). Case 2 and 3 have J_{rot} that are so small compared to J_{fly} that they can be assumed to not affect the overall rotational inertia. Case 1 on the other hand have such a

large rotor diameter that the equivalent rotational inertia of the rotor on the flywheel side of the gear box is much larger than the zero rotational inertia of the flywheel.

6 Discussion

The WEC simulations performed with the four control strategies could possibly be valid if a buoy can move according to the control strategies. The theoretical buoy used is only subjected to the vertical forces of an upward lifting force, a downward gravity force and a downward pulling line force. No considerations have been taken to the turbulence of water and the viscous damping of the short cylindrical shaped buoy as it moves through the water. If the interaction of real buoy behaviour in water were to be added to the *Simulink* model the high acceleration parts of the control strategies would possibly be affected the most due to the viscous damping. In e.g. the constant velocity control strategy the acceleration to constant velocity would take longer time than in section 4.2.3. A possible way to counteract this would be to either lower the rotational inertia of the flywheel or use a different buoy design. The first would diminish the downward pulling line force acting on the buoy and the second would diminish the viscous damping of the water acting on the buoy. For the other control strategies, the starting vertical acceleration of the buoy would possibly be lower and the acceleration part be longer. This could result in the need of diminishing the time delay or the rotational inertia of the flywheel, as previously mentioned, so that the buoy still will surface at the top of the wave.

Further, no consideration was taken to the size of the buoy compared to the wave, as the buoy was simulated as one point with the lifting force of the buoy from reference [4]. The sinusoidal waves were used mainly due to the problem of obtaining real wave data, but with the reason in mind that if the model works on simulated wave data it should possibly work on real wave data. With respect to existing wave lengths and wave amplitudes on the Swedish west coast with high energy content, the simulated wave, for all simulations in chapter 4, was chosen to be 3 meters high and 5 seconds long. The waves on the west coast with the highest energy content are between 1 and 4 meters high and between 4 and 7 seconds long.

Ideal components were assumed and thus no losses accounted for. Consequently, the 2D simulations performed in *Maxwell* does not take into account the end effects of the generator, which is quite suitable since no losses are accounted for.

The model requires knowledge of the length and amplitude of the waves in order to apply an appropriate electric torque and time delay to get a high energy uptake. This could be done by realising that the waves repeat themselves and thus is the same control strategy applied until the wave changes. Otherwise could a wave measuring buoy be placed at an arbitrary distance from the buoy, thus measuring the waves and relaying the data to a controller that applies the appropriate electric torque and time delay. If an entire WEC park were to be made just a few measuring buoys would be needed to obtain data for the WECs at the outskirts of the park. These WECs could then relay how the control strategy worked to the other WECs in an attempt to adjust the control strategy and optimize the operation for the remaining WECs in the park.

The four control strategies were chosen to see the difference in operation between keeping different quantities constant. The first to be modelled was the constant electric torque control strategy due to its simplicity, then were a bit more complex strategies such as

constant acceleration and constant velocity modelled. The fairly constant power strategy were the last to be modelled since it required the most modelling knowledge. The constant torque and constant power strategies were chosen to simulate the wave front as well as the flywheel operation, since these were considered as the control strategies that could provide the lowest maximum electric torque at the same time as keeping the electric torque fairly constant.

Figure 5.7 shows that the maximum electric torque has a close to linear dependency on the diameter of the generator over a range from about 1000 to 8000 Nm and 140 to 460 mm. Thus could an exchange ratio, for the gear box, that gives a lower torque/rpm-ratio have been used. From a generator point of view a lower ratio is more appropriate than the current torque/rpm-ratio, which is quite high (7.14 for *case 1* to 3.19 for *case 3*). Choosing $G = 100$ would have given a more appropriate electric torque of a couple of hundred Nm and thus a lower torque/rpm-ratio (0.0714 for *case 1* to 0.0319 for *case 3*).

The exchange ratios and current densities for the three designs could also have been chosen so that a maximum electric torque that is outside the plot in figure 5.7 could have been achieved. Although, there is no assurance that the dependency between the outer diameter and the torque continues to be linear outside the interval, even though there is an almost linear dependency between them on the interval.

With a pole-pair number of 5 and the maximum angular velocities in the end of section 4.4, the frequencies are, according to (5.1), around 35 Hz, which is quite low for a SG. If utilising a higher pole-pair number or having a higher angular velocity the frequency could have been made higher. A higher angular velocity implies utilising a higher gear box ratio than $G = 10$, giving a lower torque/rpm-ratio which, as previously mentioned, is wanted.

7 Conclusion

Simulations have shown that mechanical energy from a WEC may be stored in a flywheel during a wave front, and be retrieved and used between wave fronts. The control model that simulates waves and the lifting force on a buoy in it was together with the control strategy models merged into one model which gave results regarding the output effect and total energy uptake for a certain wave. The merged model and sizing method have been implemented that gives a hint of the size and maximum electrical torque of a generator design for a certain simulated wave. Consequently, three generator designs have shown the importance of smoothing of the electrical torque with a flywheel, since it results in a more efficient use of material due to the need of smaller generators. The three designs with electrical torques of 1348, 1497 and 2919 Nm have shown the relative difference in size that can be obtained, and that the maximum electric torque and the material used can be more than halved between the designs.

The use of a flywheel can thus decrease the size of the generator needed if one allows for regulation of the angular velocity. It can also make better use of the material of the generator, by having e.g. constant electric torque which gives approximately constant current and hence a high copper utilisation.

8 Future work

For further development of the simple WEC model used in this thesis, the model could be connected with other models. One such model should take into account the buoy's movement in water due to viscous damping and the turbulence of water. Thus could it be investigated how a buoy should be shaped in order to accelerate, when submerged, according to the control strategies applied in this thesis. This would probably demand an alteration and tuning of the control strategies, in order to implement a model that simulates a buoy behaviour which is close to the WEC model presented here.

Models that take into account the mechanical losses with a buoy, line, freewheel, flywheel, gear box and the connection of them should also be performed. Except for the mechanical losses is a model that can calculate the output power from the generator and the losses therein needed. Taking into account all losses, both electrical and mechanical, an overall efficiency could be obtained.

The simulation of a WEC park would constitute the basic knowledge needed to see if a controller can choose the appropriate electric torque and time delay to get a high energy uptake by receiving relayed data from wave measuring buoys or other WECs. The use of a wave measuring buoy is suggested in reference [4].

References

[1] *Vågkraftsprojekt - Lysekil* (2011) http://www.el.angstrom.uu.se/forskningsprojekt/WavePower/Lysekilsprojektet.html (2012-04-23)

[2] *Seabased* (2012) http://www.seabased.com (2012-04-23)

[3] *Ocean Energy Centre* (2012) http://www.oceanenergycentre.org (2012-04-23)

[4] Leijon M., Boström C. and others (2008) *"Wave Energy from the North Sea: Experiences from the Lysekil Research Site"*, Surveys in Geophysics, Volume 29 2008 :221–240

[5] Waters R., Engström J. and others (2009) *"Wave climate off the Swedish west coast"*, Renewable Energy 34, 1600–1606

[6] *Waves4Power* (2012) http://www.waves4power.com/ (2012-05-30)

[7] *Minesto* (2012) http://www.minesto.com/ (2012-05-30)

[8] *Ocean harvesting* (2012) http://www.oceanharvesting.com/ (2012-05-30)

[9] Serway R.A. & Jewett J.W., Jr. (2004) *"Physics for scientists and engineers with modern physics"* , 6th edition, Brooks/Cole, Belmont, Calif.

[10] Hendershot J.R. & Miller T.J.E. (2010) *"Design of brushless permanent-magnet machines"* Motor Design Books LLC, Florida, USA

[11] Hughes A. (2006) *"Electric Motors and Drives"*, 3rd edition, Newnes, Oxford

[12] Du-Bar C. (2011) *"Design of an axial flux machine for an in-wheel motor application"*, Chalmers Reproservice, Göteborg

[13] Hendershot J.R. & Miller T.J.E. (1994) *"Design of brushless permanent-magnet motors"* Magna Physics Publishing and Clarendon Press, Oxford

[14] Bianchi N. (2005) *"Electrical machine analysis using finite elements"* Taylor & Francis, Boca Raton

[15] Furlani E.P. (2001) *"Permanent magnet and electromechanical devices [electronic resource] : materials, analysis, and applications"* Academic, San Diego, Calif. ; London

[16] *Permanent Magnet Design Guidelines* (2010) http://www.magnetsales.com/Design/DesignG.htm (2012-02-27)

[17] Harnefors L. (2002) *"Control of Variable-Speed Drives"*, Mälardalen University, Västerås

[18] Gottlieb, I.M. (1997) *"Practical electric motor handbook"*, Newnes, Oxford

[19] Waters R. (2008) *"Energy from Ocean Waves: Full Scale Experimental Verification of a Wave Energy Converter"*, Comprehensive Summaries of Uppsala Dissertations from the Faculty of Science and Technology 580, ISBN 978-91-554-7354-9

[20] Engström J., Eriksson M. and others (2009) *"Wave energy converter with enhanced amplitude response at frequencies coinciding with Swedish west coast sea states by use of a supplementary submerged body"*, JOURNAL OF APPLIED PHYSICS 106, 064512

A Equivalent rotational inertia

As the energy possible to be stored in a rotating inertia depends on ω^2, see (2.11), the rotational inertia of the rotor on the secondary side is equivalent to G^2J on the primary side of the gear box, with the gear G. This relationship is confirmed in the following example, where τ is the electric torque, ω is the angular velocity, α is the angular acceleration and J is the rotational inertia and the sub indices 1 and 2 represents the primary and secondary side of the gearbox, respectively.

Statement: $G^2J_2 = J_1$

Assume: $G = n$, $\tau_1 = x$ Nm and that ω_1 goes from 0 to y rad/s in t s

$\implies \tau_2 = x/n$ Nm, $\alpha_1 = \partial\omega_1/\partial t = y/t$ rad/s^2 and $\alpha_2 = ny/t$ rad/s^2

Using $\tau = J\dfrac{\partial\omega}{\partial t} = J\alpha \implies J_1 = \dfrac{\tau_1}{\alpha_1} = xt/y$ kgm^2 and $J_2 = \dfrac{\tau_2}{\alpha_2} = xt/(n^2y)$ kgm^2

Checking with the first statement: $G^2J_2 = J_1 \implies n^2xt/(n^2y) = xt/y$